

Multi-level Cross-modal Alignment for Image Clustering

Liping Qiu*, Qin Zhang*, Xiaojun Chen†, Shaotian Cai

Shenzhen University, Shenzhen, China

qiuliping2021@email.szu.edu.cn, {qinzhang, xjchen}@szu.edu.cn, cai.st@foxmail.com

Abstract

Recently, the cross-modal pretraining model has been employed to produce meaningful pseudo-labels to supervise the training of an image clustering model. However, numerous erroneous alignments in a cross-modal pretraining model could produce poor-quality pseudo labels and degrade clustering performance. To solve the aforementioned issue, we propose a novel **Multi-level Cross-modal Alignment** method to improve the alignments in a cross-modal pre-training model for downstream tasks, by building a smaller but better semantic space and aligning the images and texts in three levels, i.e., instance-level, prototype-level, and semantic-level. Theoretical results show that our proposed method converges, and suggests effective means to reduce the expected clustering risk of our method. Experimental results on five benchmark datasets clearly show the superiority of our new method.

Introduction

Image clustering which groups images into different clusters without labels is an essential task in unsupervised learning. Many methods are proposed to utilize the large-scale pre-training models such as Resnet (He et al. 2016) or ViT (Dosovitskiy et al. 2020) to extract high-quality representations for image clustering (Ji, Vedaldi, and Henriques 2019; Li et al. 2021; Zhong et al. 2021; Wu et al. 2019; Van Gansbeke et al. 2020; Dang et al. 2021). Then, to unsupervised classification models, multiple indirect loss functions are used (e.g. sample relations (Chang et al. 2017a), invariant information (Ji, Vedaldi, and Henriques 2019; Li et al. 2021), mutual information (Wu et al. 2019) and entropy (Huang, Gong, and Zhu 2020; Van Gansbeke et al. 2020; Li et al. 2021). However, as pointed out in (Cai et al. 2023), the aforementioned techniques have difficulties in handling examples that are semantically different but visually comparable by focusing only on images.

Recently, many vision-language pre-training (VLP) models have been developed to align images and texts into a unified semantic space (Li et al. 2019; Chen et al. 2020; Ramesh et al. 2021; Li et al. 2020; Radford et al. 2021; Jia et al.

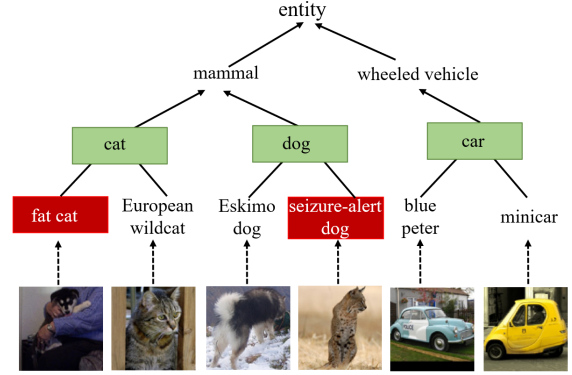


Figure 1: The nearest noun (selected from WorldNet (Miller 1995)) for the images in STL10, where the image and text embeddings are obtained via CLIP (Zhou et al. 2021). The green words correspond to the correct alignments, while the red words indicate incorrect alignments.

2021). To utilize the VLP models for image clustering, Cai et al. (Cai et al. 2023) proposed to use CLIP (Radford et al. 2021) to produce meaningful pseudo-labels and achieved significant improvements on a wide range of datasets in comparison with conventional image clustering methods. Li et al. (Li, Savarese, and Hoi 2022) also used CLIP for a zero-shot image classification task. The success of these methods suggests a promising direction for image clustering. However, as shown in Figure 1, there are instances where the alignments between images and texts in CLIP may be incorrect for downstream tasks, resulting in substandard pseudo-labels and poor clustering performance. SIC (Cai et al. 2023) simply uses CLIP to obtain the embeddings of images and texts and cannot deal with incorrect alignments. Although MUST (Li, Savarese, and Hoi 2022) strives to optimize the image encoder in CLIP, its efficiency is hampered by using the pretraining task to update the image encoder, resulting in a slow process.

To address the above problem, we propose a novel method, namely **Multi-level Cross-modal Alignment (MCA)**, an efficient way to improve the alignments between images and texts in CLIP for clustering tasks. In general, our main contributions are as follows:

*These authors contributed equally.

†Corresponding author.

- We propose to use the hierarchical structure in WordNet (see Figure 1) to filter irrelevant words and construct a smaller but better semantic space, thus reducing the affection of unrelated nouns for clustering. Our experimental findings demonstrate that it can reduce the number of words by up to 60% and significantly enhance clustering performance compared to SIC.
- We propose to optimize both image and text embeddings for downstream tasks, by aligning the images and texts at three levels, i.e., instance-level, prototype-level, and semantic-level. Our proposed method can better fix the incorrect alignments in CLIP for downstream tasks compared to SIC and MUST.
- Theoretical findings demonstrate that our proposed method converges at a sublinear rate and offers effective strategies for lowering the expected clustering risk of our method. These findings will provide valuable guidance for the design of new image clustering methods.
- Experimental results on five benchmark datasets clearly show the superiority of our new method, especially when dealing with complex clusters.

Related Work

Early deep clustering methods simply combine representation learning and shallow clustering (Xie, Girshick, and Farhadi 2016; Yang et al. 2017; Tian, Zhou, and Guan 2017; Shaham and Stanton 2018). With the rapid development of the pre-training paradigm, many methods employ large-scale pre-training models such as Resnet (He et al. 2016) or ViT (Dosovitskiy et al. 2020) to extract high-quality representations and train a classification model, by maximizing the consistency between each image and its augmentation-s/neighbors (Ji, Vedaldi, and Henriques 2019; Li et al. 2021; Zhong et al. 2021; Wu et al. 2019; Van Gansbeke et al. 2020; Zhong et al. 2021; Dang et al. 2021), or generating pseudo-labels (Wu et al. 2019; Van Gansbeke et al. 2020). However, as pointed out in (Cai et al. 2023), it is challenging for the aforementioned techniques to handle examples that are semantically different but visually comparable by only accessing visual information in images.

Cross-modal clustering has made significant progress in recent years, which usually learns a shared subspace such that the mutual agreement between multiple modalities is maximized, by Canonical Correlation Analysis (CCA) (Gao et al. 2020) or mutual information optimization (Mao et al. 2021). However, these methods require image-text pairs as input, which may be cost-intensive to collect in real applications.

Recently, vision-language pre-training (VLP) models that align multi-modal data in common feature space by different pre-training tasks have been proposed. For example, VisualBert (Li et al. 2019), UNITER (Chen et al. 2020) and DALL-E (Ramesh et al. 2021) use language-based training strategies, including mask LM (Language Modeling) such as Masked Language/Region Modeling, or autoregressive LM such as image caption and text-grounded image generation. CLIP (Radford et al. 2021) and ALIGN (Jia et al. 2021) utilize cross-modal contrastive learning to align the visual and

textual information into a unified semantic space.

Since VLP captures the relationships among images and texts (low-level semantics), it is natural to utilize VLP models to compensate for the semantic information for better image clustering. Cai et al. (Cai et al. 2023) proposed to use CLIP (Radford et al. 2021) to generate meaningful pseudo-labels for image clustering. Li et al. (Li, Savarese, and Hoi 2022) also proposed to use CLIP for zero-shot image classification tasks.

Notation and Problem Definition

Suppose we have an image dataset $\mathcal{X} = \{x_1, x_2, \dots, x_n\}$ with n instances sampled i.i.d. from input space \mathcal{D} , we can obtain the embeddings of these images as $\mathcal{U} = \{\mathbf{u}_1, \mathbf{u}_2, \dots, \mathbf{u}_n\}$ where $\mathbf{u}_i = e_I(x_i) \in \mathbb{R}^{d \times 1}$ is obtained via the image encoder $e_I(\cdot)$ of CLIP, where d is the embedding dimension. To capture the semantic meaning of these images, we first introduce a noun vocabulary $\mathcal{T} = \{t_1, t_2, \dots, t_m\}$ that includes m noun phrases sampled from WordNet (Miller 1995). Then we can obtain the embeddings of these m words as $\mathcal{V} = \{\mathbf{v}_1, \mathbf{v}_2, \dots, \mathbf{v}_m\}$ where $\mathbf{v}_i = e_T(s_i) \in \mathbb{R}^{d \times 1}$, s_i is a sentence like “A photo of a $\{t_i\}$ ” and $e_T(\cdot)$ is the text encoder of CLIP. Let c be the number of categories, our goal is to group the images in \mathcal{X} into c clusters with the help of CLIP. Let $f_I(e_I(\mathcal{X}); \phi)$ denotes the image classification network with parameters ϕ that maps an image x_i into a soft cluster assignment probability vector $\mathbf{q}_i \in \mathbb{R}^{c \times 1}$, and $f_S(e_T(\mathcal{T}); \theta)$ denotes the text classification network with parameters θ that maps a word t_i into a soft cluster assignment probability vector $\mathbf{p}_i \in \mathbb{R}^{c \times 1}$. Notably, e_I and e_T in CLIP are kept frozen during the training process.

Method

In this paper, we propose our new method which is shown in Figure 2. This new method mainly consists of three components: 1) **Semantic space construction** builds a proper semantic space \mathcal{T} , 2) **Image consistency learning** performs the consistency learning in image space, and 3) **Multi-level cross-modal alignment** aligns images and texts at three distinct levels: instance-level, prototype-level, and semantic-level. This comprehensive alignment approach significantly improves the clustering performance on downstream tasks.

Semantic Space Construction

Constructing a proper semantic space \mathcal{T} from WordNet (Miller 1995) such that the images can be well represented by the words in \mathcal{T} is very important for image clustering, because too small \mathcal{T} may lose important relevant words but too large \mathcal{T} may contain too many irrelevant noisy words. In this step, we first build a candidate semantic space \mathcal{W} as 82,000 nouns in the WordNet dataset (Miller 1995). Considering an image dataset usually makes up a small part of semantics, we propose a two-step filtering strategy to construct a proper semantic space for an image dataset: 1) **Uniqueness-based filtering** selects γ_r nearest words for each of c image cluster centers obtained by k -means of the most unique nouns whose uniqueness

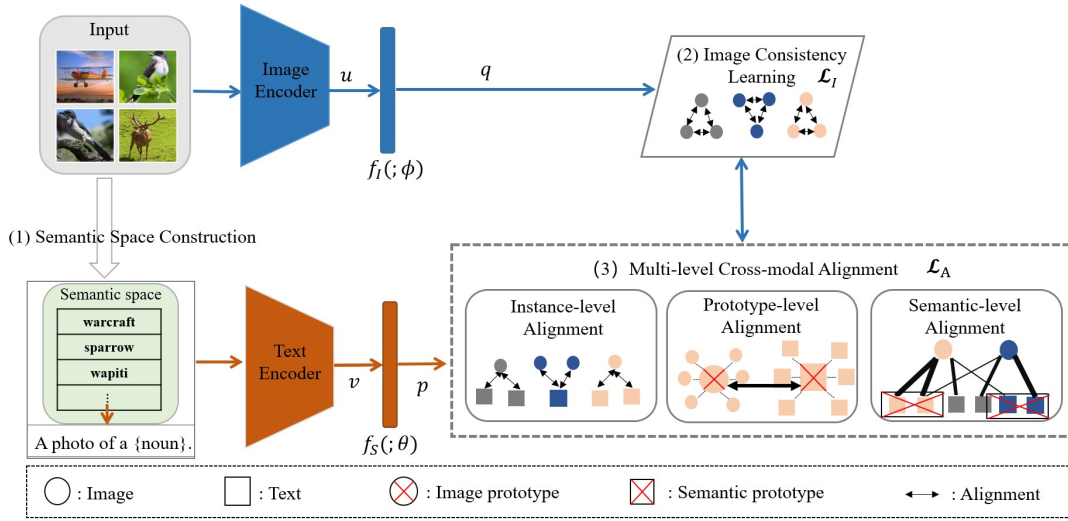


Figure 2: The framework of MCA consists of three parts: (1) Semantic space construction. (2) Image consistency learning (3) Multi-level cross-modal alignment. The thickness of lines in adaptive instance-level alignment reflects the magnitude of attention scores.

scores (Cai et al. 2023) are greater than a given hyperparameter ρ_u . 2) **Hierarchy-based filtering** employs the hierarchical structure in WordNet to further filter \mathcal{W}_c to form the final semantic space \mathcal{T} . Let $\mathcal{T} = \emptyset$. Given an image x_i , we find its nearest noun $w_i \in \mathcal{W}_c$ and search its hierarchical structure from WordNet (Miller 1995) to form a hierarchical semantic tree. In general, the words in the lower layers provide more fine-grained information for distinguishing the images, while the words in the higher layers may be useless for clustering. Figure 1 shows, for example, “mammal” is the common parent of “dog” and “cat” and cannot distinguish the images in “dog” or “cat”. Therefore, we propose a hierarchy-based filtering strategy that filters out the top γ_h levels (excluding root node) and add each of the remaining words into \mathcal{T} if it is also in \mathcal{W}_c .

Image Consistency Learning

Intuitively, an image and its nearest images may have similar soft cluster assignments. Therefore, we propose the following loss function for image consistency learning:

$$\mathcal{L}_I(f_I(e_I(\mathcal{X}); \phi)) = -\frac{1}{n} \sum_{i=1}^n \sum_{j=rn(\mathcal{N}_{k_I}^I(x_i))} \log \mathbf{q}_i^T \mathbf{q}_j - \eta \sum_{l=1}^c \bar{q}_l \log \bar{q}_l \quad (1)$$

where $\mathcal{N}_{k_I}^I(x_i)$ contains k_I nearest images of x_i and $rn(\mathcal{N}_{k_I}^I(x_i))$ randomly selects a sample from $\mathcal{N}_{k_I}^I(x_i)$. The second item is the popular negative entropy loss for preventing trivial solutions that most samples belong to a small proportion of clusters, where $\bar{q}_l = \frac{\sum_{i=1}^n q_{il}}{n}$ is the average cluster assignment. η is a trade-off parameter.

Multi-level Cross-modal Alignment

When using a cross-modal pretraining model for image clustering, the main challenge is to rectify incorrect alignments between images and words in image data. In this paper, we propose a novel **Multi-level Cross-modal Alignment** method for this task, which is shown in Figure 2. Specifically, our method employs a three-level alignment approach. Firstly, at the **Instance-level Alignment**, each image is aligned with its neighboring texts. Secondly, the **Prototype-level Alignment** aligns each image prototype with its nearest text prototype. Lastly, at the **Semantic-level Alignment**, each image is aligned with its neighboring texts in the semantic space. The detailed descriptions of these three alignment processes are provided below.

Instance-level alignment: Given an image x_i and its neighboring texts $\mathcal{N}_{k_S}^S(x_i)$, we propose the following contrastive loss function to facilitate the alignment:

$$\mathcal{L}_{ia} = -\frac{1}{n} \sum_{i=1}^n \sum_{j=rn(\mathcal{N}_{k_S}^S(x_i))} \log \frac{\exp(\mathbf{q}_i^T \mathbf{p}_j / \tau_{ia})}{\sum_{l=1, l \neq j}^m \exp(\mathbf{q}_i^T \mathbf{p}_l / \tau_{ia})} \quad (2)$$

where τ_{ia} is a temperature parameter.

Prototype-level alignment: Instance-level alignment may be affected by noisy neighborhood relationships, so we further propose to align images and texts at prototype level which is more robust to noisy texts. We first compute an image prototype set \mathcal{H}^I , where $\mathbf{h}_l^I \in \mathcal{H}^I$ is computed as $\mathbf{h}_l^I = \frac{1}{\|\mathbf{q}_l\|_1} \sum_{i=1}^n q_{il} \mathbf{u}_i$. Then, for each image prototype $\mathbf{h}_l^I \in \mathcal{H}^I$, we can identify the word in \mathcal{T} that is closest to \mathbf{h}_l^I and finally construct a prototype set \mathcal{H}^S . To further improve the prototypes in \mathcal{H}^S , we find k_p nearest neighborhoods for each $\mathbf{h}_l^S \in \mathcal{H}^S$ to compute the prototype of these neighborhoods and replace \mathbf{h}_l^S to update \mathcal{H}^S .

Finally, to align images and texts at the prototype level, we propose the following loss function:

$$\mathcal{L}_{pa} = -\frac{1}{c} \sum_{j=1}^c \log \frac{\exp(f_I(\mathbf{h}_j^I, \phi)^T f_S(\mathbf{h}_j^S, \theta) / \tau_{pa})}{\sum_{l=1, l \neq j}^c \exp(f_I(\mathbf{h}_l^I, \phi)^T f_S(\mathbf{h}_l^S, \theta) / \tau_{pa})} \quad (3)$$

where τ_{pa} is a temperature parameter.

Semantic-level alignment: Given an image x_i and its neighbouring texts $\mathcal{N}_{k_S}^S(x_i)$, we let $\mathbf{v}_j = e_T(s_j)$ be the embeddings of $t_j \in \mathcal{N}_{k_S}^S(x_i)$ and s_j is a sentence like ‘‘A photo of a $\{t_j\}$ ’’, and $\mathbf{p}_j = f_S(\mathbf{v}_j, \theta)$. It makes sense that the neighboring texts of an image can help determine the cluster assignment of this image. Note that the alignment relationships between images and texts may vary in different downstream tasks, we propose to use the attention mechanism (Vaswani et al. 2017) to quantify the correlations between an image and its neighboring texts. Specifically, we compute \mathbf{p}'_i as the weighted combination of the neighboring texts’ assignments as:

$$\begin{aligned} \mathbf{p}'_i &= f_A(\mathbf{u}_i, \mathbf{V}^S, \mathbf{P}^S; \mathbf{W}^I, \mathbf{W}^S) \\ &= \sum_{j \in \mathcal{N}_{k_S}^S(x_i)} \text{softmax}((\mathbf{W}^I \mathbf{u}_i)^T \mathbf{W}^S \mathbf{v}_j) \mathbf{p}_j \end{aligned} \quad (4)$$

where $f_A(\dots; \mathbf{W}^I, \mathbf{W}^S)$ is the attention network to quantify the correlations between an image and its neighboring texts and $\mathbf{W}^I, \mathbf{W}^S \in \mathbb{R}^{d \times d}$ are two parameter matrices. Then we use the argmax operation to generate one-hot pseudo-label for x_i as:

$$\mathbf{q}'_i = \text{one-hot}(c, \text{argmax}_l p'_{il}) \quad (5)$$

where $\text{one-hot}(c, l)$ generates a c -bit one-hot vector with the l -th element as 1.

Here, \mathbf{q}'_i can be considered as the semantic cluster assignment of x_i . Therefore, we perform alignment for each image x_i by aligning the semantic cluster assignment \mathbf{q}'_i to the image cluster assignment \mathbf{q}_i with the following loss function:

$$\mathcal{L}_{sa} = \frac{1}{n} \sum_{i=1}^n CE(\mathbf{q}_i, \mathbf{q}'_i) \quad (6)$$

where $CE(\cdot)$ is the cross entropy function.

The overall alignment loss function is:

$$\begin{aligned} \mathcal{L}_A(f_I(e_I(\mathcal{X}); \phi), f_S(e_T(\mathcal{T}); \theta), f_A(\dots; \mathbf{W}^I, \mathbf{W}^S)) \\ = \mathcal{L}_{ia} + \lambda_{pa} \mathcal{L}_{pa} + \lambda_{sa} \mathcal{L}_{sa} \end{aligned} \quad (7)$$

where λ_{pa} and λ_{sa} are two trade-off parameters.

The Overall Objective

We denote $\mathcal{L}_A(f_I(e_I(\mathcal{X}); \phi), f_S(e_T(\mathcal{T}); \theta), f_A(\dots; \mathbf{W}^I, \mathbf{W}^S))$ as $\mathcal{L}(g(\mathcal{S}; \varphi))$ for simplicity, where $\mathcal{S} = (\mathcal{X}, \mathcal{T})$, $\varphi = (\phi, \theta, \mathbf{W}^I, \mathbf{W}^S)$ and g consists of f_I , f_S and f_A . Finally, the overall objective can be formulated as

$$\mathcal{L}(g(\mathcal{S}; \varphi)) = \mathcal{L}_I(g(\mathcal{S}; \varphi)) + \lambda_a \mathcal{L}_A(g(\mathcal{S}; \varphi)) \quad (8)$$

where λ_a is a trade-off parameter.

Theoretical Analysis

In this part, we first analyze the convergence of our proposed method and then analyze its expected clustering risk. We first introduce the following assumptions:

Assumption 1 Image Neighborhood Consistency Bound: $\forall x_i \in \mathcal{X}, x_j \in \mathcal{N}_{k_I}^I(x_i), \mathbf{q}_i^T \mathbf{q}_j \in [\mu_I, 1]$.

Assumption 2 Cross-modal Neighborhood Consistency Bound: $\forall x_i \in \mathcal{X}, t_j \in \mathcal{N}_{k_S}^S(x_i), \mathbf{q}_i^T \mathbf{p}_j \in [\mu_C, 1]$.

Assumption 3 Image Prediction Confidence Bound: $\forall x_i \in \mathcal{X}, \|\mathbf{q}_i\|_\infty \leq \mu_p$.

Assumption 4 Image Neighborhood Imbalance Bound: $\forall x_i \in \mathcal{X}, x_i$ is in at most k'_I samples’ (in \mathcal{X}) nearest neighborhoods.

We first give the following theorem demonstrating that the optimization algorithm theoretically converges to the local optima in a sublinear speed.

Theorem 5 Suppose that $g(\mathcal{S}; \varphi)$ is twice differential with bounded gradients and Hessians, and $\mathcal{L}(g(\mathcal{S}; \varphi))$ has L -Lipschitz continuous gradient. Suppose that the learning rate η_φ satisfies $\eta_\varphi = \min\{1, \frac{C}{\sqrt{T}}\}$ for some $C > 0$, such that $\frac{C}{\sqrt{T}} \geq L$. Then our proposed method can achieve $\min_{0 \leq t \leq T} \mathbb{E} [\|\nabla \mathcal{L}(g(\mathcal{S}); \varphi^{(t)})\|_2^2] \leq \epsilon$ in $\mathcal{O}(1/\epsilon^2)$ steps, where ϵ is a very small positive real number.

Next, we analyze the ability of our method to achieve cluster performance on unseen data. Let $\hat{\mathcal{L}}_n(g)$ be the empirical clustering risk of MCA and its expectation can be denoted as $\mathcal{L}(g)$. The family of g is defined as \mathcal{G} . Then we can obtain the following theorem by analyzing the generalization bound of our proposed method.

Theorem 6 Suppose $f_I(\cdot; \phi)$ is Lipschitz smooth with constant L_I and $\|\mathbf{u}\|_\infty \leq M_u$. Suppose $\beta(\frac{1}{n} \sum_{i=1}^n q_{ii} \mathbf{u}_i) = f_I(\mathbf{h}^I, \phi)^T f_S(\mathbf{h}^S, \theta)$ is L_{IS} -Lipschitz continuous, where \mathbf{h}^I and \mathbf{h}^S are computed according to the method in Section . For any $0 < \delta < 1$, we can guarantee that with a probability of at least $1 - \delta$ for any $g \in \mathcal{G}$, the following inequality holds.

$$\mathcal{L}(g) \leq \hat{\mathcal{L}}_n(g) + \frac{\tilde{c}_1}{\sqrt{n}} + \tilde{c}_2 \sqrt{\frac{1}{2n} \log \delta^{-1}} + \frac{2dL_{IS}M_u}{n\tau_{pa}}.$$

where $\tilde{c}_1 = 2\mu_I^{-1} + 2\eta C + \frac{2\lambda_a m / \tau_{ia}}{2\lambda_a \lambda_{pa} d L_{IS} M_u / \tau_{pa}} + \frac{2\lambda_a \lambda_{sa} c \log \mu_p^{-1}}{2\lambda_a \lambda_{sa} c \log \mu_p^{-1}}$ and $\tilde{c}_2 = (2 + 2k'_I) \log \mu_I^{-1} + \eta C + \frac{2\lambda_a(1-\mu_C)}{\tau_{ia}} + \frac{\lambda_a \lambda_{pa} \frac{dcL_I M_u^2}{\tau_{pa}}}{2\lambda_a \lambda_{sa} c \log \mu_p^{-1}}$ are constants dependent on $\{n, m, \mu_I, \mu_C, \mu_p, k'_I, c, L_{IS}, L_I, M_u, d, C\}$. C is a constant.

Theorem 6 shows that our proposed method, with high probability $1 - \delta$, is with a bounded expected clustering risk on the unseen data. To summarize, the expected clustering risk of MCA is theoretically guaranteed in clustering

tasks. Note that the margin $\mathcal{L}(g) - \hat{\mathcal{L}}_n(g)$ is inversely proportional to μ_I and μ_C which reflect the neighborhood consistency in both image domain and cross-domain, and μ_p which reflects the prediction confidence, indicating that improving the neighborhood consistency in both image domain and cross-domain and prediction confidence reduces the expected risk of MCA. Meanwhile, the margin $\mathcal{L}(g) - \hat{\mathcal{L}}_n(g)$ is proportional to k'_I which reflects the neighborhood overlapping in the image domain, indicating that reducing the neighborhood imbalance (e.g., by setting a smaller number of neighbors k_I or filtering neighborhoods to reduce neighborhood imbalance) also reduces the expected risk of MCA.

Experiments and Analysis

In this section, experiments are conducted on five image benchmark datasets to validate the effectiveness of our proposed method.

Experimental Setup

Benchmarks and implementation details. We used the followfive benchmark datasets in our experiment: STL10 (Coates, Ng, and Lee 2011), Cifar10 (Krizhevsky 2009), Cifar100-20 (Krizhevsky 2009), ImageNet-Dogs (Chang et al. 2017b) and Tiny-ImageNet (Le and Yang 2015).

Evaluation Metrics. We used three evaluation metrics to evaluate clustering results, including clustering Accuracy (ACC), Normalized Mutual Information (NMI) (McDaid, Greene, and Hurley 2011), and Adjusted Rand Index (ARI) (Hubert and Arabie 1985). For these metrics, a higher value means better performance.

Comparisons with State-of-the-arts

Setup. We took the entire list of nouns in the WordNet dataset (Miller 1995) to form an initial semantic dataset for filtering which contains more than 82, 000 nouns. To evaluate the effectiveness of our proposed method, we compare it with 27 state-of-the-art clustering methods on the five datasets. For SC (Zelnik-Manor 2005), NMF (Cai et al. 2009), AE (Bengio et al. 2006), DAE (Vincent et al. 2010), DCGAN (Radford, Metz, and Chintala 2015) and VAE (Kingma and Welling 2013), the clustering results were obtained by k -means. In addition, to better represent the generalization properties of our methods for novel unseen examples, we used the same train and validation splits as those in SCAN (Van Gansbeke et al. 2020) and SIC (Cai et al. 2023). We repeated the training five times independently on each dataset and reported their mean and standard deviation values. The nearest neighbors were searched through Faiss Library (Johnson, Douze, and Jégou 2021).

Results. The comparison results with the state-of-the-art methods in terms of ACC, NMI, and ARI are presented in Tabel 1. From this table, we can observe that our method outperforms all other methods on five benchmark datasets. Especially, MCA improves ACC, NMI, and ARI by 2.8%, 1.3%, and 1.5% on Cifar100-20, and 6.6%, 3.3%, and 5.7% on ImageNet-Dogs, demonstrating that MCA better amend

the incorrect alignments and thus achieve significant performance improvement. Especially for fine-grained images such as Imagenet-dogs whose categories are difficult to distinguish, our method can provide good clustering assistance information for them through the alignment strategy. Our method can give useful clustering support information for images through the three alignment strategy, especially for fine-grained images like ImageNet-Dogs whose categories are difficult to distinguish.

Ablation Studies

Semantic space construction.

We first conduct an experiment on Cifar10 and ImageNet-Dogs to verify the effectiveness of our semantic space construction method and show the results in Table 2. The results demonstrate that **hierarchy-based filtering** can significantly enhance the semantic space compared to **uniqueness-based filtering**, especially when dealing with complex clusters that are challenging to distinguish, such as those in the ImageNet-Dogs dataset.

Loss components effectiveness. We perform an ablation analysis on ImageNet-Dogs to measure the importance of four loss components in our model, i.e., image consistency loss \mathcal{L}_I , instance-level alignment loss \mathcal{L}_{ia} , prototype-level alignment loss \mathcal{L}_{pa} and semantic-level alignment \mathcal{L}_{sa} . The results are shown in Tabel 3, indicating that each of the four components plays an important role. The integration of three cross-modal alignment strategies significantly enhances the clustering performance, even obtaining 28.1%, 23.8%, and 29.3% performance gains when all three strategies are simultaneously used. Among the three cross-modal alignment strategies, introducing semantic-level alignment yields the most significant improvement in clustering performance, indicating that operating at the semantic level can effectively address incorrect alignments. These results confirm the effectiveness of our proposed cross-modal alignment methods.

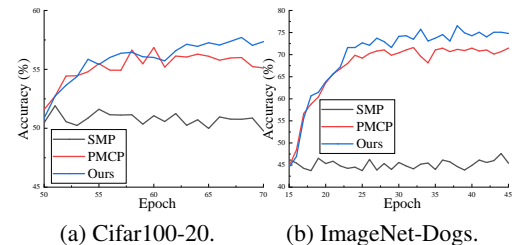


Figure 3: The average accuracy of 10 runs of pseudo-labels with epochs on Cifar100-20 and ImageNet-Dogs evolves.

Comparison of three pseudo-label generation methods.

In our method, semantic-level cross-modal alignment can be considered self-training with cross-modal pseudo-labels. To verify the effectiveness of our method, we compared three pseudo-label generation methods implemented in our framework: 1) Single Modal Pseudo-labeling (SMP) that directly generates one-hot pseudo-labels via the argmax operation on the soft cluster assignments only from images, 2) Prototype Mapping based Cross-modal Pseudo-labeling (PMCP,

Dataset	STL10			Cifar10			Cifar100-20			ImageNet-Dogs			Tiny-ImageNet		
Metrics	ACC	NMI	ARI	ACC	NMI	ARI	ACC	NMI	ARI	ACC	NMI	ARI	ACC	NMI	ARI
<i>k</i> -means (MacQueen 1967)	19.2	12.5	6.1	22.9	8.7	4.9	13.0	8.4	2.8	10.5	5.5	2.0	2.5	6.5	0.5
SC (Zelnik-Manor 2005)	15.9	9.8	4.8	24.7	10.3	8.5	13.6	9.0	2.2	11.1	3.8	1.3	2.2	6.3	0.4
NMF (Cai et al. 2009)	18.0	9.6	4.6	19.0	8.1	3.4	11.8	7.9	2.6	11.8	4.4	1.6	2.9	7.2	0.5
JULE (Yang, Parikh, and Batra 2016)	27.7	18.2	16.4	27.2	19.2	13.8	13.7	10.3	3.3	13.8	5.4	2.8	3.3	10.2	0.6
SAE (Ng et al. 2011)	32.0	25.2	16.1	29.7	24.7	15.6	15.7	10.9	4.4	—	—	—	—	—	—
DAE (Vincent et al. 2010)	30.2	22.4	15.2	29.7	25.1	16.3	15.1	11.1	4.6	19.0	10.4	7.8	3.9	12.7	0.7
AE (Bengio et al. 2006)	30.3	25.0	16.1	31.4	23.4	16.9	16.5	10.0	4.7	18.5	10.4	7.3	4.1	13.1	0.7
VAE (Kingma and Welling 2013)	28.2	20.0	14.6	29.1	24.5	16.7	15.2	10.8	4.0	17.9	10.7	7.9	3.6	11.3	0.6
DEC (Xie, Girshick, and Farhadi 2016)	35.9	27.6	18.6	30.1	25.7	16.1	18.5	13.6	5.0	19.5	12.2	7.9	3.7	11.5	0.7
ADC (Haeusser et al. 2018)	53.0	—	—	32.5	—	—	16.0	—	—	—	—	—	—	—	—
DeepCluster (Caron et al. 2018)	33.4	—	—	37.4	—	—	18.9	—	—	—	—	—	—	—	—
DAC (Chang et al. 2017a)	47.0	36.6	25.6	52.2	40.0	30.1	23.8	18.5	8.8	27.5	21.9	11.1	6.6	19.0	1.7
DDC (Chang et al. 2019)	48.9	37.1	26.7	52.4	42.4	32.9	—	—	—	—	—	—	—	—	—
DCCM (Wu et al. 2019)	48.2	37.6	26.2	62.3	49.6	40.8	32.7	28.5	17.3	38.3	32.1	18.2	10.8	22.4	3.8
IIC (Ji, Vedaldi, and Henriques 2019)	59.6	49.6	39.7	61.7	51.1	41.1	25.7	22.5	11.7	—	—	—	—	—	—
PICA (Huang, Gong, and Zhu 2020)	71.3	61.1	53.1	69.6	59.1	51.2	33.7	31.0	17.1	35.2	35.2	20.1	9.8	27.7	4.0
GCC (Zhong et al. 2021)	78.8	68.4	63.1	85.6	76.4	72.8	47.2	47.2	30.5	52.6	49.0	36.2	13.8	34.7	7.5
CC (Li et al. 2021)	85.0	76.4	72.6	79.0	70.5	63.7	42.9	43.1	26.6	42.9	44.5	27.4	14.0	34.0	7.1
TCL (Li et al. 2022)	86.8	79.9	75.7	88.7	81.9	78.0	53.1	52.9	35.7	64.4	62.3	51.6	—	—	—
SCAN* (Avg±Std)	75.5±2.0	65.4±1.2	59.0±1.6	81.8±0.3	71.2±0.4	66.5±0.4	42.2±3.0	44.1±1.0	26.7±1.3	55.6±1.5	58.7±1.3	42.8±1.3	41.1±0.5	69.4±0.3	32.7±0.4
SCAN† (Avg±Std)	76.7±1.9	68.0±1.2	61.6±1.8	87.6±0.4	78.7±0.5	75.8±0.7	45.9±2.7	46.8±1.3	30.1±2.1	59.2±0.2	60.8±0.4	45.3±0.4	—	—	—
SCAN† (Best) (Van Gansbeke et al. 2020)	80.9	69.8	64.6	88.3	79.7	77.2	50.7	48.6	33.3	59.3	61.2	45.7	42.0	69.8	33.2
NNM (Dang et al. 2021)	76.8±1.2	66.3±1.3	59.6±1.5	83.7±0.3	73.7±0.5	69.4±0.6	45.9±0.2	48.0±0.4	30.2±0.4	58.6±1.5	60.4±0.5	44.9±0.2	37.8±0.1	66.3±0.1	27.1±0.1
SIC (direct) (Avg±Std)	95.5±0.1	92.7±0.2	91.1±0.2	78.3±0.1	74.3±0.1	66.9±0.1	51.3±0.1	53.9±0.1	36.8±0.1	59.0±0.2	57.7±1.8	41.1±3.2	55.7±0.8	77.4±0.1	44.9±0.6
SIC (center-based) (Avg±Std)	96.7±0.1	93.7±0.1	93.2±0.1	91.8±0.1	83.4±0.1	83.1±0.1	54.0±0.1	54.4±0.4	38.6±0.4	61.8±1.1	63.9±1.9	49.8±1.4	61.0±0.2	80.4±0.1	51.2±0.2
SIC (adjusted center-based) (Avg±Std)	98.1±0.1	95.3±0.1	95.9±0.1	92.6±0.1	84.7±0.1	84.4±0.1	58.3±0.1	59.03±0.1	43.9±0.1	69.7±1.1	69.0±1.6	55.8±1.5	60.2±0.3	79.4±0.1	49.4±0.2
SIC (Best) (Cai et al. 2023)	98.1	95.4	95.9	92.67	84.8	84.6	58.4	59.3	44.0	71.3	71.8	58.6	61.2	80.5	51.4
Our method (Avg±Std)	98.1±0.1	95.5±0.1	96.0±0.1	92.7±0.2	84.9±0.2	84.6±0.2	59.7±0.9	59.8±0.5	44.0±0.9	74.9±2.5	73.3±1.5	61.6±2.5	61.2±0.5	79.7±0.7	51.9±0.8
Our method (Best)	98.2	95.5	96.0	92.8	85.0	84.9	61.2	60.6	45.5	77.9	75.1	64.3	61.9	81.1	52.3

Table 1: Clustering results on five benchmark datasets. The best results are highlighted in bold.

Steps	Cifar10	ImageNet-Dogs
UF	91.4	65.3
UF+HF	91.9	71.8

Table 2: Ablation studies of semantic space construction (we did not report the clustering results without filtering because the number of initial words is too large. **UF: Uniqueness-based filtering**, **HF: Hierarchy-based filtering**).

Loss Components				Result		
\mathcal{L}_I	\mathcal{L}_{ia}	\mathcal{L}_{pa}	\mathcal{L}_{sa}	ACC	NMI	ARI
✓				46.7±0.5	48.9±0.7	32.6±0.5
✓		✓	✓	66.0±3.4	67.7±2.5	50.7±4.1
✓	✓		✓	63.5±2.5	69.7±2.1	52.7±3.5
✓	✓	✓		53.1±3.8	55.4±2.8	37.4±2.4
✓	✓	✓	✓	74.8±2.7	72.7±2.0	61.9±2.5

Table 3: Ablation studies on ImageNet-Dogs.

is the adjusted center-based method in (Cai et al. 2023)) that generates pseudo-labels from the prototype level alignments in the original CLIP, and 3) **Ours** that generates pseudo-labels by simultaneously learning relationships among images and neighboring texts, while also updating the image and text embeddings. The comparison results on Cifar100-20 and ImageNet-Dogs are shown in Figure 3, demonstrating that our method significantly outperforms the other two methods on both datasets. These results indicate that learning adaptive relationships at the semantic level substantially improves the quality of pseudo-labels.

Figure 4 shows an example of our proposed pseudo-label generation method. In this example, we select an example from each of the three classes and three neighboring words for each image. Although these exist irrelevant neighboring words for an image, our method can identify irrelevant

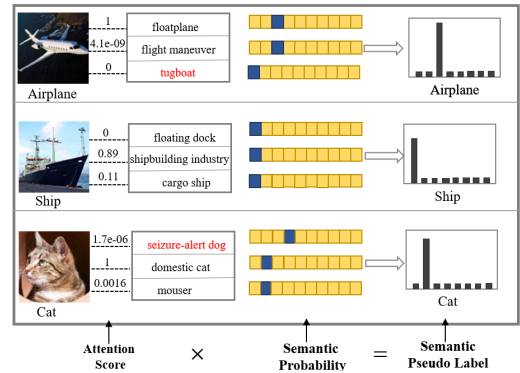


Figure 4: Example of pseudo-label generation in MCA. The words below (on the right side of) the images are ground-truth/ neighboring labels and the red color indicates irrelevant texts. The blue block in the semantic probability indicates the class the left word is assigned to (with the largest probability).

words and eliminate the affection of incorrect alignments in CLIP.

Sensitivity Analysis

Sensitivity on neighborhood parameters k_S and k_p in cross-modal alignment. In our alignment method, k_S controls the number of neighboring texts in the instance-level and semantic-level alignments, and k_p controls the number of neighboring texts to recompute the semantic prototype in the prototype-level alignment. Figures 5a and 5b show that too large k_S causes performance degeneration due to the introduction of irrelevant texts. Figures 5c and 5d show that k_p does not change the performance too much.

Sensitivity on trade-off parameters η , λ_a , λ_{pa} and λ_{sa} . Figure 6 shows the sensitivity analysis of trade-off parameters η , λ_a , λ_{pa} and λ_{sa} . From these figures, we can observe

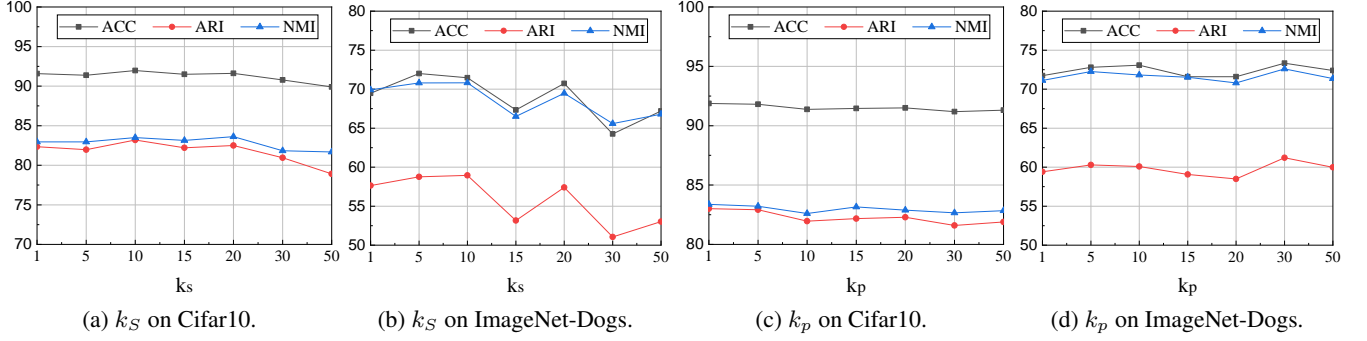


Figure 5: Sensitivity analysis of k_S and k_p .

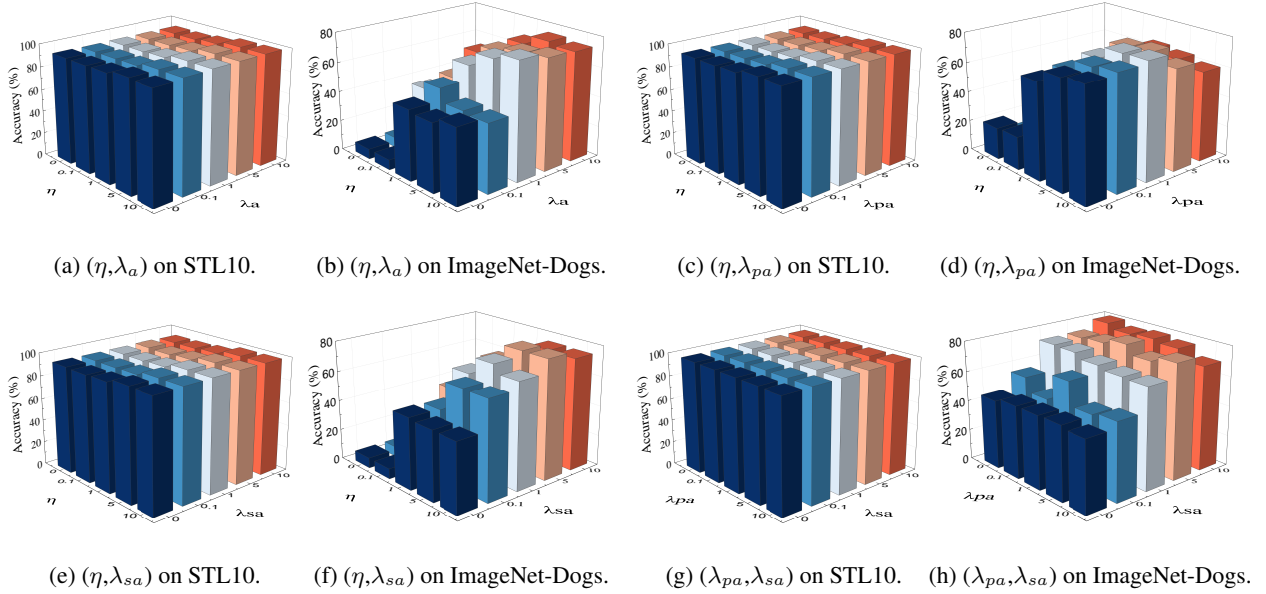


Figure 6: Sensitivity analysis of trade-off parameters η , λ_a , λ_{pa} and λ_{sa} .

that the performance of our method does not change too much with the change of four parameters on STL10. However, in ImageNet-Dogs, we can see that the performance of our method improves with increasing values of η , λ_{pa} , and λ_{sa} . In particular, our method appears to be more sensitive to changes in λ_{sa} than λ_{pa} on ImageNet-Dogs.

Time Costs

The training durations of SIC/MUST/MCA were approximately 0.5/2/1 hours on STL10, 1.5/6.5/3 hours on CIFAR10, 3/11.5/5 hours on CIFAR100-20, 0.5 / 1.7 / 1 hours on ImageNet-Dogs and 4/18/5 on Tiny-ImageNet. While it is true that our method generates a smaller semantic space, it does require the training of three networks, which can result in a longer training time compared to SIC. However, our method is much more efficient than MUST.

Conclusion

We have proposed a novel method to address the incorrect alignments in CLIP for image clustering. Our method includes the construction of a proper semantic space and a multi-level cross-modal alignment approach for aligning images and texts in downstream tasks at three levels. Theoretical results have shown interesting insights, and experimental results have demonstrated the superiority of our method. However, we acknowledge that our method may not be as cost-effective as SIC, as it involves three types of alignments. The proper setting of hierarchy levels also remains a challenge that needs further investigation. Additionally, our method exhibits lower performance compared to MUST, primarily due to the absence of class names. For future work, we will focus on enhancing the performance of our method and exploring new avenues for improvement. Leveraging the theoretical results to augment our method holds promise and will be a key research direction we pursue.

Acknowledgments

This work is jointly supported by Major Project of the New Generation of Artificial Intelligence under Grant no.2018AAA0102900; in part by NSFC under Grant no. 92270122 and no.62206179; and in part by Guangdong Provincial Natural Science Foundation under Grant no. 2023A1515012584 and no.2022A1515010129; and in part by the Shenzhen Research Foundation for Basic Research, China, under Grant JCYJ20210324093000002; and in part by University stability Support program of Shenzhen under Grant no.20220811121315001.

References

- Bengio, Y.; Lamblin, P.; Popovici, D.; and Larochelle, H. 2006. Greedy layer-wise training of deep networks. In *Proceedings of neural information processing systems*, 153–160.
- Cai, D.; He, X.; Wang, X.; Bao, H.; and Han, J. 2009. Locality Preserving Nonnegative Matrix Factorization. In *Proceedings of IJCAI 2009*, 1010–1015.
- Cai, S.; Qiu, L.; Chen, X.; Zhang, Q.; and Chen, L. 2023. Semantic-Enhanced Image Clustering. In *Proceedings of the AAAI Conference on Artificial Intelligence*, 6869–6878.
- Caron, M.; Bojanowski, P.; Joulin, A.; and Douze, M. 2018. Deep clustering for unsupervised learning of visual features. In *Proceedings of the European conference on computer vision (ECCV)*, 132–149.
- Chang, J.; Guo, Y.; Wang, L.; Meng, G.; Xiang, S.; and Pan, C. 2019. Deep Discriminative Clustering Analysis. *ArXiv*, abs/1905.01681.
- Chang, J.; Wang, L.; Meng, G.; Xiang, S.; and Pan, C. 2017a. Deep Adaptive Image Clustering. In *Proceedings of the IEEE international conference on computer vision*, 5880–5888.
- Chang, J.; Wang, L.; Meng, G.; Xiang, S.; and Pan, C. 2017b. Deep Adaptive Image Clustering. In *Proceedings of ICCV 2017*, 5880–5888.
- Chen, Y.-C.; Li, L.; Yu, L.; El Kholy, A.; Ahmed, F.; Gan, Z.; Cheng, Y.; and Liu, J. 2020. Uniter: Universal image-text representation learning. In *European conference on computer vision*, 104–120. Springer.
- Coates, A.; Ng, A.; and Lee, H. 2011. An Analysis of Single-Layer Networks in Unsupervised Feature Learning. In *Proceedings of AISTATS 2011*, volume 15, 215–223.
- Dang, Z.; Deng, C.; Yang, X.; Wei, K.; and Huang, H. 2021. Nearest Neighbor Matching for Deep Clustering. In *Proceedings of the IEEE/CVF Conference on Computer Vision and Pattern Recognition*, 13693–13702.
- Dosovitskiy, A.; Beyer, L.; Kolesnikov, A.; Weissenborn, D.; Zhai, X.; Unterthiner, T.; Dehghani, M.; Minderer, M.; Heigold, G.; Gelly, S.; et al. 2020. An image is worth 16x16 words: Transformers for image recognition at scale. *arXiv preprint arXiv:2010.11929*.
- Gao, Q.; Lian, H.; Wang, Q.; and Sun, G. 2020. Cross-modal subspace clustering via deep canonical correlation analysis. In *Proceedings of the AAAI Conference on Artificial Intelligence*, 3938–3945.
- Haeusser, P.; Plapp, J.; Golkov, V.; Aljalbout, E.; and Cremers, D. 2018. Associative deep clustering: Training a classification network with no labels. In *Proceedings of GCPR 2018*, 18–32.
- He, K.; Zhang, X.; Ren, S.; and Sun, J. 2016. Deep residual learning for image recognition. In *Proceedings of the IEEE conference on computer vision and pattern recognition*, 770–778.
- Huang, J.; Gong, S.; and Zhu, X. 2020. Deep Semantic Clustering by Partition Confidence Maximisation. In *Proceedings of the IEEE/CVF conference on computer vision and pattern recognition*, 8846–8855.
- Hubert, L.; and Arabie, P. 1985. Comparing partitions. *Journal of Classification*, 2(1): 193–218.
- Ji, X.; Vedaldi, A.; and Henriques, J. F. 2019. Invariant Information Clustering for Unsupervised Image Classification and Segmentation. In *Proceedings of the IEEE/CVF international conference on computer vision*, 9864–9873.
- Jia, C.; Yang, Y.; Xia, Y.; Chen, Y.-T.; Parekh, Z.; Pham, H.; Le, Q.; Sung, Y.-H.; Li, Z.; and Duerig, T. 2021. Scaling up visual and vision-language representation learning with noisy text supervision. In *International Conference on Machine Learning*, 4904–4916. PMLR.
- Johnson, J.; Douze, M.; and Jégou, H. 2021. Billion-Scale Similarity Search with GPUs. *Proceedings of IEEE Transactions on Big Data*, 7(3): 535–547.
- Kingma, D. P.; and Welling, M. 2013. Auto-encoding variational bayes. *arXiv preprint arXiv:1312.6114*.
- Krizhevsky, A. 2009. Learning Multiple Layers of Features from Tiny Images. *Master's thesis, University of Tront*.
- Latała, R.; and Oleszkiewicz, K. 1994. On the best constant in the Khinchin-Kahane inequality. *Studia Mathematica*, 109(1): 101–104.
- Le, Y.; and Yang, X. 2015. Tiny imagenet visual recognition challenge. *CS 231N*, 7(7): 3.
- Li, J.; Savarese, S.; and Hoi, S. C. 2022. Masked unsupervised self-training for zero-shot image classification. *arXiv preprint arXiv:2206.02967*.
- Li, L. H.; Yatskar, M.; Yin, D.; Hsieh, C.-J.; and Chang, K.-W. 2019. Visualbert: A simple and performant baseline for vision and language. *arXiv preprint arXiv:1908.03557*.
- Li, W.; Gao, C.; Niu, G.; Xiao, X.; Liu, H.; Liu, J.; Wu, H.; and Wang, H. 2020. Unimo: Towards unified-modal understanding and generation via cross-modal contrastive learning. *arXiv preprint arXiv:2012.15409*.
- Li, Y.; Hu, P.; Liu, Z.; Peng, D.; Zhou, J. T.; and Peng, X. 2021. Contrastive clustering. In *Proceedings of the AAAI Conference on Artificial Intelligence*, 8547–8555.
- Li, Y.; Yang, M.; Peng, D.; Li, T.; Huang, J.; and Peng, X. 2022. Twin contrastive learning for online clustering. *International Journal of Computer Vision*, 130(9): 2205–2221.
- MacQueen, J. 1967. Some methods for classification and analysis of multivariate observation. *Proceedings of the 5th Berkeley Symposium on Mathematical Statistics and Probability*, 281–297.

- Mao, Y.; Yan, X.; Guo, Q.; and Ye, Y. 2021. Deep mutual information maximin for cross-modal clustering. In *Proceedings of the AAAI Conference on Artificial Intelligence*, 8893–8901.
- McDaid, A. F.; Greene, D.; and Hurley, N. 2011. Normalized mutual information to evaluate overlapping community finding algorithms. *arXiv preprint arXiv:1110.2515*.
- Miller, G. A. 1995. WordNet: a lexical database for English. *Communications of the ACM*, 38(11): 39–41.
- Mohri, M.; Rostamizadeh, A.; and Talwalkar, A. 2018. *Foundations of machine learning*. MIT press.
- Ng, A.; et al. 2011. Sparse autoencoder. *CS294A Lecture notes*, 72(2011): 1–19.
- Radford, A.; Kim, J. W.; Hallacy, C.; Ramesh, A.; Goh, G.; Agarwal, S.; Sastry, G.; Askell, A.; Mishkin, P.; Clark, J.; et al. 2021. Learning transferable visual models from natural language supervision. In *International Conference on Machine Learning*, 8748–8763. PMLR.
- Radford, A.; Metz, L.; and Chintala, S. 2015. Unsupervised representation learning with deep convolutional generative adversarial networks. *arXiv preprint arXiv:1511.06434*.
- Ramesh, A.; Pavlov, M.; Goh, G.; Gray, S.; Voss, C.; Radford, A.; Chen, M.; and Sutskever, I. 2021. Zero-shot text-to-image generation. In *International Conference on Machine Learning*, 8821–8831. PMLR.
- Shaham, U.; and Stanton, K. 2018. SpectralNet: Spectral Clustering using Deep Neural Networks. In *Proceedings of International Conference of Learning Representation*, 1–20.
- Tian, K.; Zhou, S.; and Guan, J. 2017. DeepCluster: A General Clustering Framework Based on Deep Learning. In *Proceedings of ECML PKDD 2017*, 809–825.
- Van Gansbeke, W.; Vandenhende, S.; Georgoulis, S.; Proesmans, M.; and Van Gool, L. 2020. SCAN: Learning to Classify Images Without Labels. In *Proceedings of European conference on computer vision*, 268–285.
- Vaswani, A.; Shazeer, N.; Parmar, N.; Uszkoreit, J.; Jones, L.; Gomez, A. N.; Kaiser, Ł.; and Polosukhin, I. 2017. Attention is all you need. *Advances in neural information processing systems*, 30.
- Vincent, P.; Larochelle, H.; Lajoie, I.; Bengio, Y.; and Manzagol, P.-A. 2010. Stacked denoising autoencoders: Learning useful representations in a deep network with a local denoising criterion. *JMLR*, 11(12).
- Wu, J.; Long, K.; Wang, F.; Qian, C.; Li, C.; Lin, Z.; and Zha, H. 2019. Deep Comprehensive Correlation Mining for Image Clustering. In *Proceedings of the IEEE/CVF international conference on computer vision*, 8149–8158.
- Xie, J.; Girshick, R.; and Farhadi, A. 2016. Unsupervised Deep Embedding for Clustering Analysis. In *Proceedings of International conference on machine learning*, 478–487.
- Yang, B.; Fu, X.; Sidiropoulos, N. D.; and Hong, M. 2017. Towards K-means-friendly Spaces: Simultaneous Deep Learning and Clustering. In *Proceedings of international conference on machine learning*, volume 70, 3861–3870.
- Yang, J.; Parikh, D.; and Batra, D. 2016. Joint Unsupervised Learning of Deep Representations and Image Clusters. In *Proceedings of the IEEE conference on computer vision and pattern recognition*, 5147–5156.
- Zelnik-Manor, L. 2005. Self-tuning spectral clustering. In *Proceedings of NIPS 2005*, volume 17, 1601–1608.
- Zhong, H.; Wu, J.; Chen, C.; Huang, J.; Deng, M.; Nie, L.; Lin, Z.; and Hua, X.-S. 2021. Graph contrastive clustering. In *Proceedings of the IEEE/CVF International Conference on Computer Vision*, 9224–9233.
- Zhou, K.; Yang, J.; Loy, C. C.; and Liu, Z. 2021. Learning to prompt for vision-language models. *arXiv preprint arXiv:2109.01134*.

Appendix

In this appendix, we provide detailed proof of the theoretical results.

Proof of Theorem 5

Proof 1 For simplicity, we denote $\mathcal{L}(g(\mathcal{S}); \varphi)$ as $\mathcal{L}(\varphi)$. The update rule can be formulated as

$$\varphi^{(t+1)} = \varphi^{(t)} - \eta_\varphi (\nabla \mathcal{L}(\varphi^{(t)}) + \zeta^{(t)}),$$

where $\zeta^{(t)} = \nabla \mathcal{L}(\varphi^{(t)})|_{\mathcal{B}} - \nabla \mathcal{L}(\varphi^{(t)})$ and \mathcal{B} consists of a mini-batch images sampled i.i.d from \mathcal{X} and texts sampled i.i.d from the neighbors in \mathcal{T} of these images. This indicates that $\mathbb{E}[\zeta^{(t)}] = 0$ holds. Let $\|\zeta^{(t)}\|^2 \leq \sigma^2$. First, we have

$$\begin{aligned} & \mathcal{L}(\varphi^{(t+1)}) - \mathcal{L}(\varphi^{(t)}) \\ & \leq \langle \nabla \mathcal{L}(\varphi^{(t)}), \varphi^{(t+1)} - \varphi^{(t)} \rangle + \frac{L}{2} \|\varphi^{(t+1)} - \varphi^{(t)}\|_2^2 \\ & = \langle \nabla \mathcal{L}(\varphi^{(t)}), -\eta_\varphi [\nabla \mathcal{L}(\varphi^{(t)}) + \zeta^{(t)}] \rangle + \frac{L\eta_\varphi^2}{2} \|\nabla \mathcal{L}(\varphi^{(t)}) + \zeta^{(t)}\|_2^2 \\ & = -(\eta_\varphi - \frac{L\eta_\varphi^2}{2}) \|\nabla \mathcal{L}(\varphi^{(t)})\|_2^2 + \frac{L\eta_\varphi^2}{2} \|\zeta^{(t)}\|_2^2 - (\eta_\varphi - L\eta_\varphi^2) \langle \nabla \mathcal{L}(\varphi^{(t)}), \zeta^{(t)} \rangle. \end{aligned}$$

Therefore,

$$\begin{aligned} & (\eta_\varphi - \frac{L\eta_\varphi^2}{2}) \|\nabla \mathcal{L}(\varphi^{(t)})\|_2^2 \\ & \leq \mathcal{L}(\varphi^{(t)}) - \mathcal{L}(\varphi^{(t+1)}) + \frac{L\eta_\varphi^2}{2} \|\zeta^{(t)}\|_2^2 - (\eta_\varphi - L\eta_\varphi^2) \langle \nabla \mathcal{L}(\varphi^{(t)}), \zeta^{(t)} \rangle. \end{aligned}$$

Taking summation on both sides, we have

$$\begin{aligned} & \sum_{t=1}^T (\eta_\varphi - \frac{L\eta_\varphi^2}{2}) \|\nabla \mathcal{L}(\varphi^{(t)})\|_2^2 \\ & \leq \mathcal{L}(\varphi^{(1)}) - \mathcal{L}(\varphi^{(T+1)}) + \frac{L\eta_\varphi^2}{2} \sum_{t=1}^T \|\zeta^{(t)}\|_2^2 - \sum_{t=1}^T (\eta_\varphi - L\eta_\varphi^2) \langle \nabla \mathcal{L}(\varphi^{(t)}), \zeta^{(t)} \rangle. \end{aligned}$$

Further, taking the expectation with respect to ζ on both sides, one can find that

$$\begin{aligned} \sum_{t=1}^T (\eta_\varphi - \frac{L\eta_\varphi^2}{2}) \mathbb{E}_\zeta \|\nabla \mathcal{L}(\varphi^{(t)})\|^2 & \leq \mathcal{L}(\varphi^{(1)}) + \frac{L\eta_\varphi^2}{2} \sum_{t=1}^T \|\zeta^{(t)}\|^2 \\ & \leq \mathcal{L}(\varphi^{(1)}) + \frac{L\eta_\varphi^2 T \sigma^2}{2} \end{aligned}$$

Thus we have

$$\begin{aligned} \min_t \mathbb{E}_\zeta \|\nabla \mathcal{L}(\varphi^{(t)})\|^2 & \leq \frac{\sum_{t=1}^T (\eta_\varphi - \frac{L\eta_\varphi^2}{2}) \mathbb{E}_\zeta \|\nabla \mathcal{L}(\varphi^{(t)})\|_2^2}{\sum_{t=1}^T (\eta_\varphi - \frac{L\eta_\varphi^2}{2})} \\ & \leq \frac{2\mathcal{L}(\varphi^{(1)}) + L\eta_\varphi^2 T \sigma^2}{\sum_{t=1}^T (2\eta_\varphi - L\eta_\varphi^2)} \\ & \leq \frac{2\mathcal{L}(\varphi^{(1)}) + L\eta_\varphi^2 T \sigma^2}{T\eta_\varphi} \\ & = \frac{2\mathcal{L}(\varphi^{(1)})}{T\eta_\varphi} + L\sigma^2\eta_\varphi \\ & \leq \frac{2\mathcal{L}(\varphi^{(1)})}{T} \max\{L, \frac{\sqrt{T}}{C}\} + L\sigma^2 \min\{\frac{1}{L}, \frac{C}{\sqrt{T}}\} \\ & = \mathcal{O}(\frac{1}{\sqrt{T}}). \end{aligned}$$

Proof of Theorem 6

To prove Theorem 6, we first introduce the following lemmas.

Lemma 7 Given a set of n samples \mathcal{S} , we define the following empirical risk

$$\widehat{\mathcal{L}}_n(g) = -\frac{1}{n} \sum_{i=1}^n \log \mathbf{q}_i^T \mathbf{q}_{rn(i)},$$

and corresponding expected risk

$$\mathcal{L}(g) = -\mathbb{E} [\log \mathbf{q}^T \mathbf{q}^r].$$

where $rn(i) = rn(\mathcal{N}_{k_I}^I(x_i))$ and $rn(\mathcal{N}_{k_I}^I(x_i))$ randomly select a sample from $\mathcal{N}_{k_I}^I(x_i)$. $\mathbf{q}_i = g((x_i, \emptyset); \varphi)$ and \mathbf{q}^r is the prediction of a randomly selected sample from the neighborhood of \mathbf{q} . With probability at least $1 - \delta$, the following inequality holds

$$\mathcal{L}(g) \leq \widehat{\mathcal{L}}_n(g) + \frac{2\mu_I^{-1}}{\sqrt{n}} + 2 \log \mu_I^{-1} \sqrt{\frac{\log \delta^{-1}}{2n}}.$$

Proof 2 Let $\mathcal{S}' = (\mathcal{S} - s_j) \cup s_{j'}$. The empirical risks on \mathcal{S}' is denoted as $\widehat{\mathcal{L}}'_n(g)$. We have

$$\left| \sup_{g \in \mathcal{G}} \left| \mathcal{L}(g) - \widehat{\mathcal{L}}_n(g) \right| - \sup_{g \in \mathcal{G}} \left| \mathcal{L}(g) - \widehat{\mathcal{L}}'_n(g) \right| \right| \leq \sup_{g \in \mathcal{G}} \left| \widehat{\mathcal{L}}_n(g) - \widehat{\mathcal{L}}'_n(g) \right|,$$

According to Assumption 4, let $\{x_{j1}, x_{j2}, \dots, x_{jk'_S}\}$ be the set with x_j as neighbor. Then we have

$$\begin{aligned} \sup_{g \in \mathcal{G}} \left| \widehat{\mathcal{L}}_S(g) - \widehat{\mathcal{L}}_{S'}(g) \right| &\leq \sup_{g \in \mathcal{G}} \frac{1}{n} \left(\left| -(\log \mathbf{q}_j^T \mathbf{q}_{rn(j)} - \log \mathbf{q}_{j'}^T \mathbf{q}_{rn(j')}) \right| + \left| -\sum_{l=r1}^{rk'_S} (\log \mathbf{q}_l^T \mathbf{q}_j - \log \bar{\mathbf{q}}_l^T \bar{\mathbf{q}}_{rn(l)}) \right| \right) \\ &\leq \frac{(2 + 2k'_I) \log \mu_I^{-1}}{n}, \end{aligned}$$

where the last inequality is according to Assumption 1.

Combine the above two equations and we get:

$$\left| \sup_{f \in \mathcal{F}} \left| \mathcal{L}(f) - \widehat{\mathcal{L}}_S(f) \right| - \sup_{f \in \mathcal{F}} \left| \mathcal{L}(f) - \widehat{\mathcal{L}}_{S'}(f) \right| \right| \leq \frac{(2 + 2k'_I) \log \mu_I^{-1}}{n}.$$

Let $\{\sigma_1, \sigma_2, \dots, \sigma_n\}$ be i.i.d. independent random variables taking values in $\{-1, 1\}$ and $\bar{S} := \{\bar{s}_1, \dots, \bar{s}_n\}$ be the independent copy of S , Then we have

$$\begin{aligned} \mathbb{E}_S \left[\sup_{g \in \mathcal{G}} |\mathcal{L}(g) - \widehat{\mathcal{L}}_n(g)| \right] &\leq \mathbb{E}_{S, \bar{S}, \sigma} \left[\sup_{g \in \mathcal{G}} \frac{1}{n} \left| \sum_{i=1}^n \sigma_i (\log \mathbf{q}_i^T \mathbf{q}_{rn(i)} - \log \bar{\mathbf{q}}_i^T \bar{\mathbf{q}}_{rn(i)}) \right| \right] \\ &\leq 2 \mathbb{E}_{S, \sigma} \left[\sup_{g \in \mathcal{G}} \frac{1}{n} \left| \sum_{i=1}^n \sigma_i \log \mathbf{q}_i^T \mathbf{q}_{rn(i)} \right| \right] \\ &\leq 2 \mathbb{E}_{S, \sigma} \left[\sup_{g \in \mathcal{G}} \frac{1}{n} \left| \sum_{i=1}^n \sigma_i \left(\frac{1}{\mathbf{q}_i^T \mathbf{q}_{rn(i)}} - 1 \right) \right| \right] \\ &\leq 2 \mathbb{E}_{S, \sigma} \left[\sup_{g \in \mathcal{G}} \frac{1}{n} \left| \sum_{i=1}^n \sigma_i \frac{1}{\mathbf{q}_i^T \mathbf{q}_{rn(i)}} \right| \right] \\ &\leq 2 \mathbb{E}_S \left[\sup_{g \in \mathcal{G}} \frac{1}{n} \left(\sum_{i=1}^n \left(\frac{1}{\mathbf{q}_i^T \mathbf{q}_{rn(i)}} \right)^2 \right)^{\frac{1}{2}} \right] \\ &\leq \frac{2\mu_I^{-1}}{\sqrt{n}}. \end{aligned}$$

where the second to last inequality is obtained by Khintchine-Kahane inequality (Latała and Oleszkiewicz 1994) and the last inequality is obtained by Assumption 1.

Thus according to the McDiarmid inequality (Mohri, Rostamizadeh, and Talwalkar 2018), with probability at least $1 - \delta$ for any $g \in \mathcal{G}$, we have

$$\mathcal{L}(g) \leq \widehat{\mathcal{L}}_n(g) + \frac{2\mu_I^{-1}}{\sqrt{n}} + (2 + 2k'_I) \log \mu_I^{-1} \sqrt{\frac{\log \delta^{-1}}{2n}}.$$

Lemma 8 Given a set of n samples \mathcal{S} , we define the following empirical risk

$$\hat{\mathcal{L}}_n(g) = - \sum_{l=1}^c \left(\frac{1}{n} \sum_{i=1}^n q_{il} \right) \log \left(\frac{1}{n} \sum_{i=1}^n q_{il} \right),$$

and corresponding expected risk

$$\mathcal{L}(g) = - \sum_{l=1}^c \mathbb{E}(q^l) \log \mathbb{E}(q^l).$$

where $\mathbf{q}_i = g((x_i, \emptyset); \varphi)$. With probability at least $1 - \delta$, the following inequality holds

$$\mathcal{L}(g) \leq \hat{\mathcal{L}}_n(g) + \frac{2C}{\sqrt{n}} + C \sqrt{\frac{\log \delta^{-1}}{2n}}.$$

where $C = |\log \xi + 1|$ is a bounded constant and ξ is a constant according to the Lagrange Mean Theorem of the function $b(x) = x \log x$.

Proof 3 Let $\mathcal{S}' = (\mathcal{S} - s_j) \cup s_{j'}$. The empirical risk on \mathcal{S}' is denoted as $\hat{\mathcal{L}}'_n$. Define $b(x) = x \log x$, according to the Lagrange Mean Theorem, there exists constant ξ such that $|b(x) - b(y)| \leq |\log \xi + 1| |x - y|$. We have

$$\begin{aligned} & \left| \sup_{g \in \mathcal{G}} \left| \mathcal{L}(g) - \hat{\mathcal{L}}_n(g) \right| - \sup_{g \in \mathcal{G}} \left| \mathcal{L}(g) - \hat{\mathcal{L}}'_n(g) \right| \right| \\ & \leq \sup_{g \in \mathcal{G}} \left| \hat{\mathcal{L}}_n(g) - \hat{\mathcal{L}}'_n(g) \right| \\ & \leq \sup_{g \in \mathcal{G}} \frac{|\log \xi + 1|}{n} \sum_l^c |q_{jl} - q'_{jl}| \\ & \leq \frac{|\log \xi + 1|}{n} \\ & = \frac{C}{n}. \end{aligned}$$

where $C = |\log \xi + 1|$.

Next, we analyze the upper bound of the term $\mathbb{E}_S \left[\sup_{g \in \mathcal{G}} |\mathcal{L}(g) - \hat{\mathcal{L}}_n(g)| \right]$. Let $\sigma_1, \sigma_2, \dots, \sigma_n$ be i.i.d. independent random variables taking values in $\{-1, 1\}$ and $\bar{S} := \{\bar{s}_1, \dots, \bar{s}_n\}$ be the independent copy of $S := \{s_1, \dots, s_n\}$. Then we have

$$\begin{aligned} & \mathbb{E}_S \left[\sup_{g \in \mathcal{G}} |\mathcal{L}(g) - \hat{\mathcal{L}}_S(g)| \right] \\ & \leq \mathbb{E}_{S, \bar{S}, \sigma} \left[\sup_{g \in \mathcal{G}} \frac{1}{n} \sum_{i=1}^n \sigma_i \left(\sum_{l=1}^c |\log \xi + 1| |q_{il} - \bar{q}_{il}| \right) \right] \\ & \leq 2 |\log \xi + 1| \mathbb{E}_{S, \sigma} \left[\sup_{g \in \mathcal{G}} \frac{1}{n} \sum_{i=1}^n \sigma_i \sum_{l=1}^c q_{il} \right] \\ & \leq 2 |\log \xi + 1| \mathbb{E}_S \left[\sup_{g \in \mathcal{G}} \frac{1}{n} \left(\sum_{i=1}^n \left[\sum_{l=1}^c q_{il} \right]^2 \right)^{\frac{1}{2}} \right] \\ & \leq \frac{2 |\log \xi + 1|}{\sqrt{n}} \\ & = \frac{2C}{\sqrt{n}}. \end{aligned}$$

where the second to last inequality is obtained by Khintchine-Kahane inequality (Latała and Oleszkiewicz 1994).

Thus according to the McDiarmid inequality (Mohri, Rostamizadeh, and Talwalkar 2018), with probability at least $1 - \delta$ for any $g \in \mathcal{G}$, we have

$$\mathcal{L}(g) \leq \hat{\mathcal{L}}_n(g) + \frac{2C}{\sqrt{n}} + C \sqrt{\frac{\log \delta^{-1}}{2n}}.$$

Lemma 9 Given a set of n samples \mathcal{S} , we define the following empirical risk

$$\begin{aligned}\hat{\mathcal{L}}_n(g) &= -\frac{1}{n} \sum_{i=1}^n \log \frac{\exp(\mathbf{q}_i^T \mathbf{p}_{rn(i)}/\tau_{ia})}{\sum_{l=1, l \neq rn(i)}^m \exp(\mathbf{q}_i^T \mathbf{p}_l/\tau_{ia})} \\ &= -\frac{1}{n} \sum_{i=1}^n \left[\frac{\mathbf{q}_i^T \mathbf{p}_{rn(i)}}{\tau_{ia}} - \log \left(\sum_{l=1, l \neq rn(i)}^m \exp(\mathbf{q}_i^T \mathbf{p}_l/\tau_{ia}) \right) \right],\end{aligned}$$

and corresponding expected risk

$$\mathcal{L}(g) = -\mathbb{E} \left[\frac{\mathbf{q}^T \mathbf{p}'}{\tau_{ia}} - \log(\exp((\mathbb{E}(\mathbf{q}^T \mathbf{p}) - \mathbf{q}^T \mathbf{p}')/\tau_{ia})) \right].$$

where $rn(i) = rn(\mathcal{N}_{k_S}^S(x_i))$ randomly select a sample from $\mathcal{N}_{k_S}^S(x_i)$ and \mathbf{p}' is the prediction of a randomly selected sample from the neighborhood of \mathbf{q} . With probability at least $1 - \delta$, the following inequality holds

$$\mathcal{L}(g) \leq \hat{\mathcal{L}}_n(g) + \frac{2m}{\sqrt{n}\tau_{ia}} + \frac{2(1 - \mu_C)}{\tau_{ia}} \sqrt{\frac{\log \delta^{-1}}{2n}}.$$

Proof 4 Let $\mathcal{S}' = (\mathcal{S} - s_j) \cup s_{j'}$. The empirical risk on \mathcal{S}' is denoted as $\hat{\mathcal{L}}'_n$. We have

$$\begin{aligned}& \left| \sup_{g \in \mathcal{G}} \mathcal{L}(g) - \hat{\mathcal{L}}_n(g) - \sup_{g \in \mathcal{G}} \mathcal{L}(g) - \hat{\mathcal{L}}'_n(g) \right| \\ & \leq \sup_{g \in \mathcal{G}} \left| \hat{\mathcal{L}}_n(g) - \hat{\mathcal{L}}'_n(g) \right| \\ & \leq \sup_{g \in \mathcal{G}} \frac{1}{n} \left| \frac{\mathbf{q}_j^T \mathbf{p}_{rn(j)} - \mathbf{q}_{j'}^T \mathbf{p}_{rn(j')}}{\tau_{ia}} - \log \frac{\sum_{l=1, l \neq rn(j)}^m \exp(\mathbf{q}_j^T \mathbf{p}_l/\tau_{ia})}{\sum_{l=1, l \neq rn(j')}^m \exp(\mathbf{q}_{j'}^T \mathbf{p}_l/\tau_{ia})} \right| \\ & \leq \frac{2(1 - \mu_C)}{n\tau_{ia}}\end{aligned}$$

which is based on Assumption 2.

Next, we analyze the upper bound of the term $\mathbb{E}_S \left[\sup_{g \in \mathcal{G}} |\mathcal{L}(g) - \hat{\mathcal{L}}_n(g)| \right]$. Let $\sigma_1, \sigma_2, \dots, \sigma_n$ be i.i.d. independent random variables taking values in $\{-1, 1\}$ and $\bar{S} := \{\bar{s}_1, \dots, \bar{s}_n\}$ be the independent copy of $S := \{s_1, \dots, s_n\}$. Then we have

$$\begin{aligned}\mathbb{E}_S \left[\sup_{g \in \mathcal{G}} |\mathcal{L}(g) - \hat{\mathcal{L}}_n(g)| \right] &\leq \mathbb{E}_{S, \bar{S}, \sigma} \left[\sup_{g \in \mathcal{G}} \frac{1}{n} \sum_{i=1}^n \sigma_i \left| \frac{\mathbf{q}_i^T \mathbf{p}_{rn(i)} - (\bar{\mathbf{q}}_i^T)^T \bar{\mathbf{p}}_{rn(i)}}{\tau_{ia}} - \log \frac{\sum_{l=1, l \neq rn(i)}^m \exp(\mathbf{q}_i^T \mathbf{p}_l/\tau_{ia})}{\sum_{l=1, l \neq rn(i)}^m \exp((\bar{\mathbf{q}}_i^T)^T \bar{\mathbf{p}}_l/\tau_{ia})} \right| \right] \\ &\leq 2\mathbb{E}_{S, \sigma} \left[\sup_{g \in \mathcal{G}} \frac{1}{n} \sum_{i=1}^n \sigma_i \left| \frac{\mathbf{q}_i^T \mathbf{p}_{rn(i)}}{\tau_{ia}} - \log \left(\sum_{l=1, l \neq rn(i)}^m \exp(\mathbf{q}_i^T \mathbf{p}_l/\tau_{ia}) \right) \right| \right] \\ &\leq 2\mathbb{E}_{S, \sigma} \left[\sup_{g \in \mathcal{G}} \frac{1}{n} \sum_{i=1}^n \sigma_i \left(\left| \frac{\mathbf{q}_i^T \mathbf{p}_{rn(i)}}{\tau_{ia}} \right| + \left| \sum_{l=1, l \neq rn(i)}^m \frac{\mathbf{q}_i^T \mathbf{p}_l}{\tau_{ia}} \right| \right) \right] \\ &\leq 2\mathbb{E}_S \left[\sup_{g \in \mathcal{G}} \frac{1}{n\tau_{ia}} \left(\left(\sum_{i=1}^n (\mathbf{q}_i^T \mathbf{p}_{rn(i)})^2 \right)^{\frac{1}{2}} + \left(\sum_{i=1}^n \left(\sum_{l=1, l \neq rn(i)}^m \mathbf{q}_i^T \mathbf{p}_l \right)^2 \right)^{\frac{1}{2}} \right) \right] \\ &\leq \frac{2m}{\sqrt{n}\tau_{ia}}\end{aligned}$$

where the second to last inequality is obtained by Khintchine-Kahane inequality (Latała and Oleszkiewicz 1994) and the last inequality is obtained by Assumption 2.

Thus according to the McDiarmid inequality (Mohri, Rostamizadeh, and Talwalkar 2018), with probability at least $1 - \delta$ for any $g \in \mathcal{G}$, we have

$$\mathcal{L}(g) \leq \hat{\mathcal{L}}_n(g) + \frac{2m}{\sqrt{n}\tau_{ia}} + \frac{2(1 - \mu_C)}{\tau_{ia}} \sqrt{\frac{\log \delta^{-1}}{2n}}.$$

Lemma 10 Given a set of n samples \mathcal{S} , we define the following empirical risk

$$\widehat{\mathcal{L}}_n(g) = -\frac{1}{c} \sum_{j=1}^c \log \frac{\exp((\rho_j^I)^T \rho_j^S / \tau_{pa})}{\sum_{l=1, l \neq j}^c \exp((\rho_j^I)^T \rho_j^S / \tau_{pa})} = -\frac{1}{c} \sum_{j=1}^c \left[\frac{(\rho_j^I)^T \rho_j^S}{\tau_{pa}} - \log \left(\sum_{l=1, l \neq j}^c \exp((\rho_j^I)^T \rho_j^S / \tau_{pa}) \right) \right]$$

where $\rho^I = f_I(\mathbf{h}^I, \phi)$ and $\rho^S = f_S(\mathbf{h}^S, \theta)$. $h_l^I = \frac{\sum_{i=1}^n q_{il} \mathbf{u}_i}{\|\mathbf{q}_l\|}$ and $\mathbf{h}^S = \text{close}(\mathbf{h}^I)$ computed according to Section is close to \mathbf{h}^I .

The corresponding expected risk is defined as

$$\mathcal{L}(g) = -\frac{1}{c} \sum_{j=1}^c \left[\frac{\mathbb{E}(\rho_j^I)^T \mathbb{E}(\rho_j^S, \theta)}{\tau_{pa}} - \log \left(\sum_{l=1, l \neq j}^c \exp(\mathbb{E}(\rho_j^I)^T \mathbb{E}(\rho_l^S) / \tau_{pa}) \right) \right]$$

With probability at least $1 - \delta$, the following inequality holds

$$\mathcal{L}(g) \leq \widehat{\mathcal{L}}_n(g) + \frac{2dL_{IS}M_u}{n\tau_{pa}} + \frac{dcL_I M_u^2}{\tau_{pa}} \sqrt{\frac{\log \delta^{-1}}{2n}}.$$

Proof 5 Let $\mathcal{S}' = (\mathcal{S} - s_r) \cup s_{r'}$. The empirical risk on \mathcal{S}' is denoted as $\widehat{\mathcal{L}}'_n$. We have

$$\begin{aligned} & \left| \sup_{g \in \mathcal{G}} \left| \mathcal{L}(g) - \widehat{\mathcal{L}}_n(g) \right| - \sup_{g \in \mathcal{G}} \left| \mathcal{L}(g) - \widehat{\mathcal{L}}'_n(g) \right| \right| \\ & \leq \sup_{g \in \mathcal{G}} \left| \widehat{\mathcal{L}}_n(g) - \widehat{\mathcal{L}}'_n(g) \right| \\ & \leq \sup_{g \in \mathcal{G}} \frac{1}{c} \sum_{j=1}^c \left| \frac{(\rho_j^I)^T \rho_j^S - ((\rho')^I_j)^T (\rho')^S_j}{\tau_{pa}} - \log \frac{\sum_{l=1, l \neq j}^c \exp((\rho_j^I)^T \rho_l^S / \tau_{pa})}{\sum_{l=1, l \neq j}^c \exp(((\rho')^I_j)^T (\rho')^S_l / \tau_{pa})} \right| \\ & \leq \sup_{g \in \mathcal{G}} \frac{2}{\tau_{pa}} \max_{j \in [c]} |(\rho_j^I)^T \rho_j^S - ((\rho')^I_j)^T (\rho')^S_j| \\ & \leq \sup_{g \in \mathcal{G}} \frac{2L_{IS}}{\tau_{pa}} \max_{j \in [c]} \|\mathbf{h}_j^S - (\mathbf{h}'_j)^S\| \\ & \leq \sup_{g \in \mathcal{G}} \frac{2L_{IS}}{\tau_{pa}} \max_{j \in [c]} \left\| \frac{1}{n} (q_{rl} \mathbf{u}_r - q_{r'l} \mathbf{u}_{r'}) \right\| \\ & \leq \frac{2dL_{IS}M_u}{n\tau_{pa}} \end{aligned}$$

Next, we analyze the upper bound of the term $\mathbb{E}_S \left[\sup_{g \in \mathcal{G}} |\mathcal{L}(g) - \widehat{\mathcal{L}}_n(g)| \right]$. Let $\sigma_1, \sigma_2, \dots, \sigma_n$ be i.i.d. independent random

variables taking values in $\{-1, 1\}$ and $\bar{S} := \{\bar{s}_1, \dots, \bar{s}_n\}$ be the independent copy of $S := \{s_1, \dots, s_n\}$. Then we have

$$\begin{aligned}
\mathbb{E}_{\mathcal{S}} \left[\sup_{g \in \mathcal{G}} |\mathcal{L}(g) - \hat{\mathcal{L}}_{\mathcal{S}}(g)| \right] &\leq \mathbb{E}_{\mathcal{S}, \bar{\mathcal{S}}, \sigma} \left[\sup_{g \in \mathcal{G}} \frac{1}{c} \sum_{j=1}^c \left| \frac{(\rho_j^I)^T \rho_j^S - (\bar{\rho}_j^I)^T \bar{\rho}_j^S}{\tau_{pa}} - \log \frac{\sum_{l=1, l \neq rn(i)}^m \exp((\rho_j^I)^T \rho_l^S / \tau_{pa})}{\sum_{l=1, l \neq rn(i)}^m \exp((\bar{\rho}_j^I)^T \bar{\rho}_l^S / \tau_{pa})} \right| \right] \\
&\leq 2\mathbb{E}_{\mathcal{S}, \sigma} \left[\sup_{g \in \mathcal{G}} \frac{1}{c} \sum_{j=1}^c \left| \frac{(\rho_j^I)^T \rho_j^S}{\tau_{pa}} - \log \left(\sum_{l=1, l \neq j}^c \exp((\rho_j^I)^T \rho_l^S / \tau_{pa}) \right) \right| \right] \\
&\leq 2\mathbb{E}_{\mathcal{S}, \sigma} \left[\sup_{g \in \mathcal{G}} \frac{1}{c\tau_{pa}} \sum_{j=1}^c \left((\rho_j^I)^T \rho_j^S + \sum_{l=1, l \neq j}^c (\rho_j^I)^T \rho_l^S \right) \right] \\
&\leq 2\mathbb{E}_{\mathcal{S}, \sigma} \left[\sup_{g \in \mathcal{G}} \frac{c}{\tau_{pa}} \max_{j \in [c]} \left((\rho_j^I)^T \rho_j^S \right) \right] \\
&\leq 2\mathbb{E}_{\mathcal{S}, \sigma} \left[\sup_{g \in \mathcal{G}} \frac{cL_I}{\tau_{pa}} \max_{j \in [c]} \left\| f_I \left(\frac{\sum_{i=1}^n \sigma_i q_{ij} \mathbf{u}_i}{\|\mathbf{q}_l\|}, \phi \right)_j \right\|^2 \right] \\
&\leq 2\mathbb{E}_{\mathcal{S}, \sigma} \left[\sup_{g \in \mathcal{G}} \frac{cL_I}{\tau_{pa}} \max_{j \in [c]} \left\| \left(\frac{\sum_{i=1}^n \sigma_i q_{ij} \mathbf{u}_i}{n} \right)_j \right\|^2 \right] \\
&\leq 2\mathbb{E}_{\mathcal{S}, \sigma} \left[\sup_{g \in \mathcal{G}} \frac{cL_I}{\tau_{pa}} \max_{j \in [c]} \frac{\sum_{i=1}^n \sum_{l=1}^d (\sigma_i q_{ij} u_{il})^2}{n^2} \right] \\
&\leq \frac{dcL_I M_u^2}{\tau_{pa} n}
\end{aligned}$$

where the last inequality is obtained by assumption in Theorem 5.

Thus according to the McDiarmid inequality (Mohri, Rostamizadeh, and Talwalkar 2018), with probability at least $1 - \delta$ for any $g \in \mathcal{G}$, we have

$$\mathcal{L}(g) \leq \hat{\mathcal{L}}_n(g) + \frac{2dL_I M_u}{n\tau_{pa}} + \frac{dcL_I M_u^2}{\tau_{pa}} \sqrt{\frac{\log \delta^{-1}}{2n}}.$$

Lemma 11 Given a set of n samples \mathcal{S} , we define the following empirical risk

$$\hat{\mathcal{L}}_n(g) = -\frac{1}{n} \sum_{i=1}^n \sum_{l=1}^c q_{il} \log q'_{il},$$

and

$$\mathcal{L}(g) = -\sum_{l=1}^c \mathbb{E}(\mathbf{q})^l \log \mathbb{E}(\mathbf{q}')^l.$$

where \mathbf{q}' contains one-hot pseudo-label. With probability at least $1 - \delta$, the following inequality holds

$$\mathcal{L}(f) \leq \hat{\mathcal{L}}_n(f) + \frac{2 \log \mu_p^{-1}}{\sqrt{n}} + 2 \log \mu_p^{-1} \sqrt{\frac{\log \delta^{-1}}{2n}}.$$

Proof. Let $\mathcal{S}' = (\mathcal{S} - s_j) \cup s_{j'}$. We have

$$\begin{aligned}
&\sup_{f \in \mathcal{F}} \left| \hat{\mathcal{L}}_n(f) - \hat{\mathcal{L}}'_n(f) \right| \\
&\leq \sup_{f \in \mathcal{F}} \frac{1}{n} \left| \sum_l (q_{jl} \log q'_{jl} - q_{j'l} \log q'_{j'l}) \right| \\
&\leq \frac{2c \log \mu_p^{-1}}{n}.
\end{aligned}$$

Next we analyze the upper bound of the expectation term, i.e., $\mathbb{E}_{\mathcal{S}} \left[\sup_{f \in \mathcal{F}} |\mathcal{L}(f) - \hat{\mathcal{L}}_{\mathcal{S}}(f)| \right]$. Let $\sigma_1, \sigma_2, \dots, \sigma_n$ be i.i.d. independent random variables taking values in $\{-1, 1\}$ and $\bar{S} := \{\bar{x}_1, \dots, \bar{x}_n\}$ be the independent copy of $S := \{x_1, \dots, x_n\}$.

Then we have

$$\begin{aligned}
& \mathbb{E}_S \left[\sup_{f \in \mathcal{F}} |\mathcal{L}(f) - \hat{\mathcal{L}}_n(f)| \right] \\
&= \mathbb{E}_{S, \tilde{S}, \sigma} \left[\sup_{f \in \mathcal{F}} \frac{1}{n} \left| \sum_{i=1}^n \sigma_i \left(\sum_{l=1}^c (p_{il} \log q_{il} - \bar{p}_{il} \log \bar{q}_{il}) \right) \right| \right] \\
&\leq 2 \mathbb{E}_{S, \sigma} \left[\sup_{f \in \mathcal{F}} \frac{1}{n} \left| \sum_{i=1}^n \sigma_i \sum_{l=1}^c p_{il} \log q_{il} \right| \right] \\
&\leq 2 \mathbb{E}_{S, \sigma} \left[\sup_{f \in \mathcal{F}} \frac{1}{n} \left(\sum_{i=1}^n \left[\sum_{l=1}^c p_{il} \log q_{il} \right]^2 \right)^{\frac{1}{2}} \right] \\
&\leq \frac{2c \log \mu_p^{-1}}{\sqrt{n}}.
\end{aligned}$$

Thus according to the McDiarmid inequality (Mohri, Rostamizadeh, and Talwalkar 2018), with probability at least $1 - \delta$ for any $f \in \mathcal{F}$, we have

$$\mathcal{L}(f) \leq \hat{\mathcal{L}}_n(f) + \frac{2c \log \mu_p^{-1}}{\sqrt{n}} + 2c \log \mu_p^{-1} \sqrt{\frac{\log \delta^{-1}}{2n}}.$$

Now we give the proof of Theorem 6.

Proof 6 According to Lemma 7, 8, 9, 10 and 11, with probability at least $1 - \delta$ for any $g \in \mathcal{G}$, the empirical risk and the expected risk of the overall loss function in Eq. (8) has the following relationship

$$\mathcal{L}(g) \leq \hat{\mathcal{L}}_n(g) + \frac{\tilde{c}_1}{\sqrt{n}} + \tilde{c}_2 \sqrt{\frac{1}{2n} \log \delta^{-1}} + \frac{2dL_{IS}M_u}{n\tau_{pa}}.$$

where $\tilde{c}_1 = 2\mu_I^{-1} + 2\eta C + 2\lambda_a m/\tau_{ia} + 2\lambda_a \lambda_{ca} c \log \mu_p^{-1}$ and $\tilde{c}_2 = (2 + 2k'_I) \log \mu_I^{-1} + \eta C + \frac{2\lambda_a(1-\mu_C)}{\tau_{ia}} + \lambda_a \lambda_{sp} \frac{dcL_I M_u^2}{\tau_{pa}} + 2\lambda_a \lambda_{ca} c \log \mu_p^{-1}$. This finishes the proof.

Implementation Details

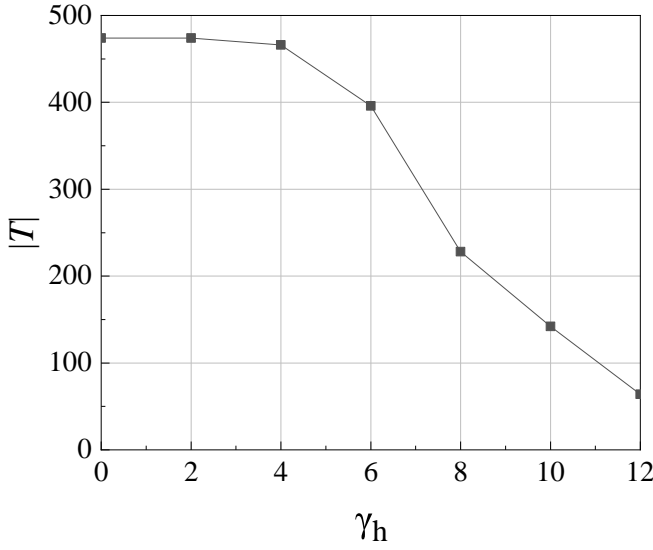
We used ViT-32 (Dosovitskiy et al. 2020) and Transformer (Vaswani et al. 2017) in CLIP as the image and text encoders, respectively. The cluster heads f_I and f_S were implemented by two $d \times c$ fully connected layers, where $d = 512$ is the embedding dimension and c is the number of clusters, respectively. Before training, all datasets were preprocessed with the augmentation method used in CLIP (Zhou et al. 2021), i.e., random square crop from resized images. We used cosine similarity to measure the similarity between image and word embeddings and thus construct the top k_I nearest image neighbors $\mathcal{N}_{k_I}^I(x_i)$ and the top k_S nearest texts $\mathcal{N}_{k_S}^S(x_i)$ for each image x_i . Epoch numbers and batch sizes of all datasets were set to 100 and 128. The nearest neighbors used in image consistency learning were searched through Faiss Library (Johnson, Douze, and Jégou 2021). All experiments were carried out on four NVIDIA GeForce RTX 2080 Tis.

Benchmark Datasets

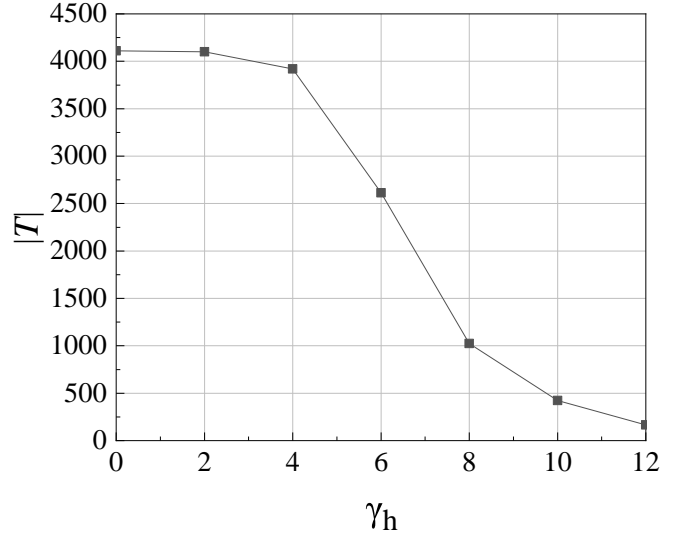
The details of five benchmark datasets are shown in Figure 4.

Table 4: Statistics of five benchmark datasets.

Dataset	Image size	#Classes	#Training	#Testing
STL10	96×96	10	5,000	8,000
Cifar10	32×32	10	50,000	10,000
Cifar100-20	32×32	20	50,000	10,000
ImageNet-Dogs	224×224	15	19,500	750
Tiny-ImageNet	64×64	200	100,000	10,000

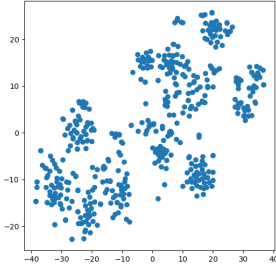


(a) Result on STL10.

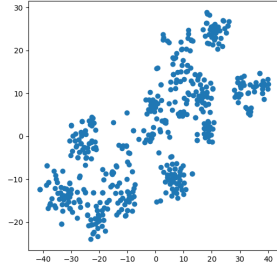


(b) Result on ImageNet-Dogs.

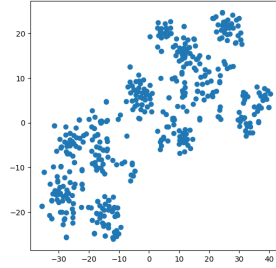
Figure 7: $|\mathcal{T}|$ versus γ_h .



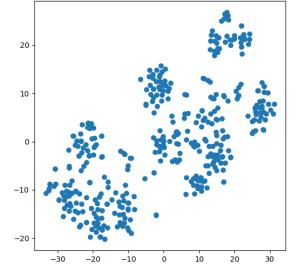
(a) $\gamma_h=0$.



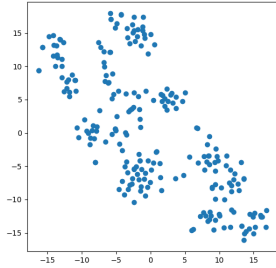
(b) $\gamma_h=2$.



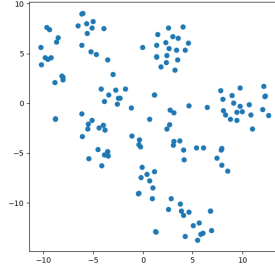
(c) $\gamma_h=4$.



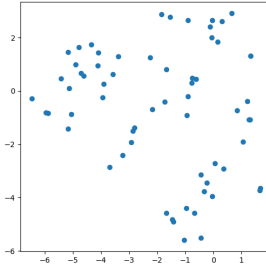
(d) $\gamma_h=6$.



(e) $\gamma_h=8$.



(f) $\gamma_h=10$.



(g) $\gamma_h=12$.

Figure 8: t -SNE visualization of the words in \mathcal{T} on STL10, with the increasing of γ_h .

Semantic Space Construction

Figures 14 and 15 show two examples of the hierarchy-based filtering results on STL-10 and ImageNet-Dogs, which are parts of the hierarchical semantic tree built from WordNet (Miller 1995). From these figures, we can observe the two hierarchical semantic trees contain more than 10 levels of words. However, we also observe that the top-level words, such as “group”, “unit” in Figures 14, are useless for distinguishing the 10 classes in STL-10. Therefore, we removed top-6 levels of words on STL-10 and top-10 levels of words on ImageNet-Dogs in our experiments. We also show the changes of $|\mathcal{T}|$ versus γ in Figure 7, indicating that the number of words in \mathcal{T} decreases quickly with the increase of γ_h . Figures 8 and 9 display the t -SNE visualization of the words in \mathcal{T} for two datasets. It is evident that, as the value of γ_h increases, the remaining words tend to preserve the structural information. We assess the effectiveness of a hierarchy-based filtering technique.

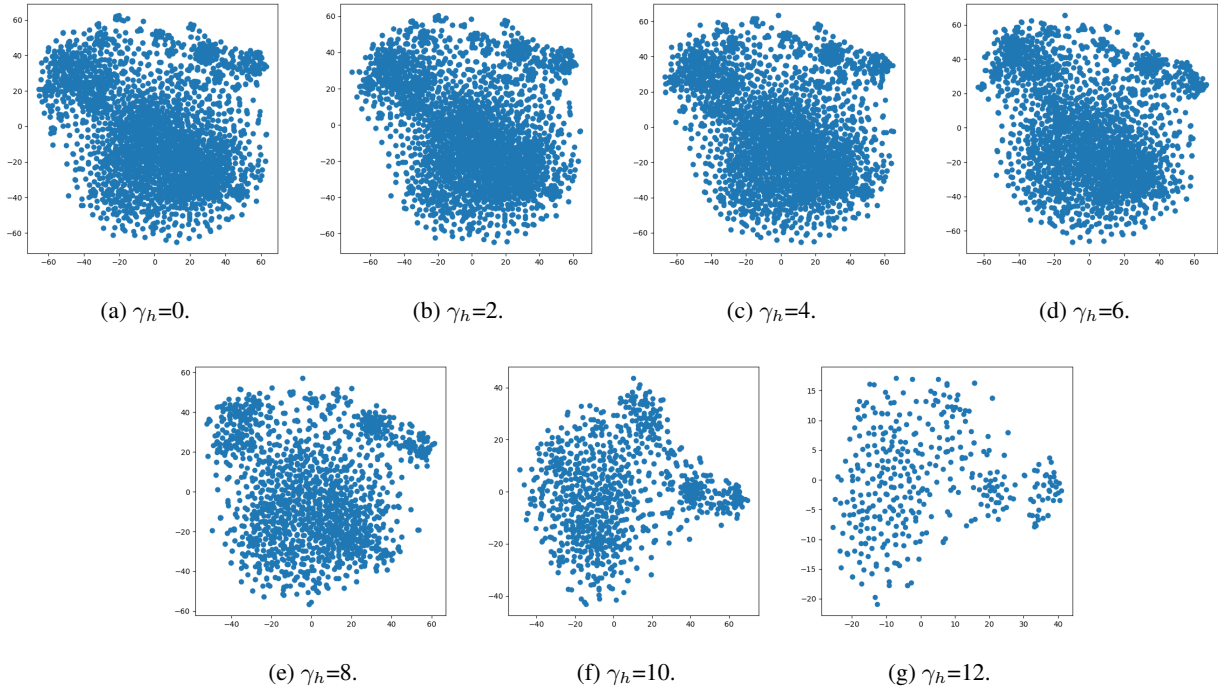


Figure 9: t -SNE visualization of the words in \mathcal{T} on ImageNet-Dogs, with the increase of γ_h .

Hyper-parameters

The hyper-parameters used on five benchmark datasets are listed in Table 5.

Table 5: The hyper-parameters used on five benchmark datasets. η_ϕ : learning rate, γ_r : the number of nearest nouns for each image center, γ_u : the number of most unique nouns, γ_h : the number of hierarchy levels in the hierarchical semantic tree (the root is level 0) to filter, k_I : the number of nearest images, k_S : the number of nearest texts, k_p : the number of nearest texts to an image center, τ_{ia} : the temperature to control the softness of instance-level alignment, τ_{pa} : the temperature to control the softness of prototype-level alignment, η , λ_a , λ_{pa} and λ_{ca} : the trade-off parameters.

Dataset	η_ϕ	γ_r	γ_u	γ_h	k_I	k_S	k_p	τ_{ia}	τ_{pa}	η	λ_a	λ_{pa}	λ_{ca}
STL10	1e-4	50	0.05	6	20	5	20	1	1	10	10	0.1	5
Cifar10	1e-3	500	0.03	12	5	5	1	0.2	0.05	1	1	1	1
Cifar100-20	1e-2	100	0.05	5	5	20	20	1	1	1	1	1	1
ImageNet-Dogs	1e-5	1000	0.05	10	5	20	30	0.05	0.6	10	1	1	5
Tiny-ImageNet	1e-3	100	0.03	5	10	5	20	1	1	1	1	1	1

Sensitivity Analysis

Sensitivity on hyperparameters γ_r and γ_h .

In our method, γ_r and γ_h are used to construct the semantic space, where γ_r controls the number of central nearest neighbors selected in WordNet, and γ_h allows further filtering of low-level semantic words. Figure 10 shows the sensitivity results of our method with respect to γ_r , indicating that a too-small γ_r leads to a loss of semantic information while a too-large γ_r leads to noise in the semantic space, resulting in a risk of cluster degradation. Therefore, we set $\gamma_r = 50$ for STL10 and $\gamma_r = 1000$ for ImageNet-Dogs.

As for γ_h , a larger γ_h removes useless words in higher levels such that the remaining words in \mathcal{T} can better distinguish the images, while a small γ_h retains enough words for clustering. Figure 11 shows the sensitivity results of our method with respect to γ_h , which indicates that too small or too large γ_h causes performance degeneration. Relatively speaking, the performance changes caused by the variation of γ_h on ImageNet-Dogs are larger than those on STL10. Finally, we set $\gamma_h = 6$ for STL10 and $\gamma_h = 10$ for ImageNet-Dogs.

Compared to Figure 7, we can observe that our method produces the best results when retaining about $[400, 500]$ words in \mathcal{T} on both datasets.

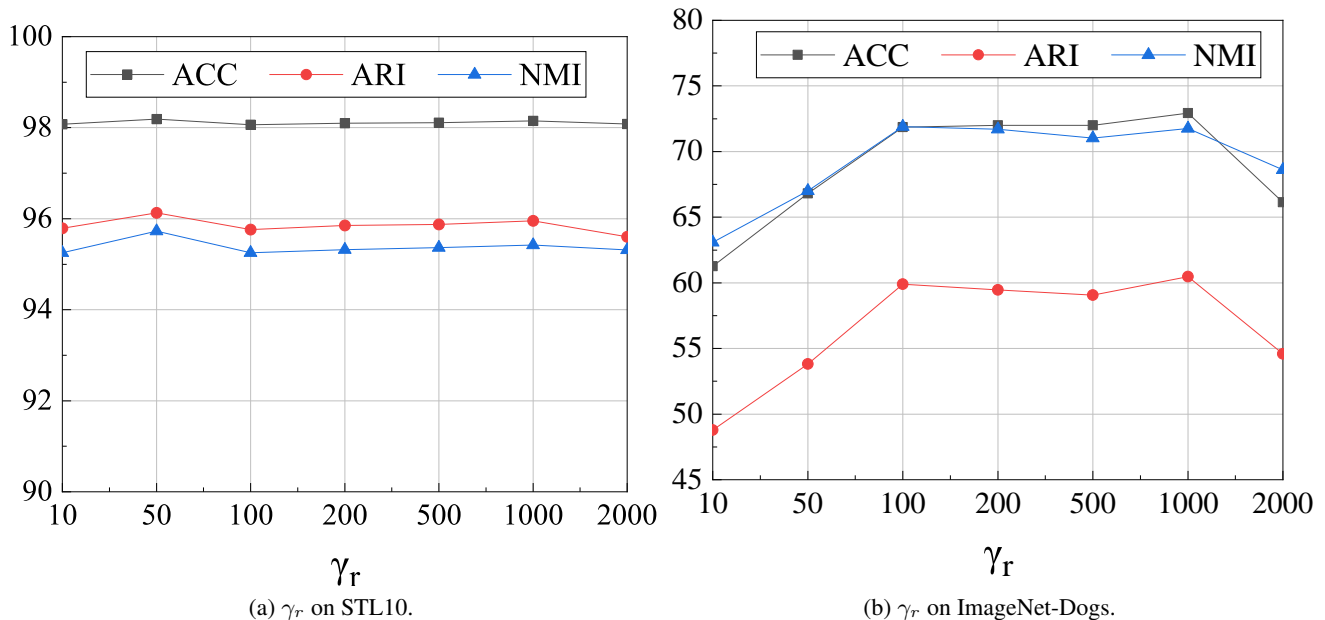
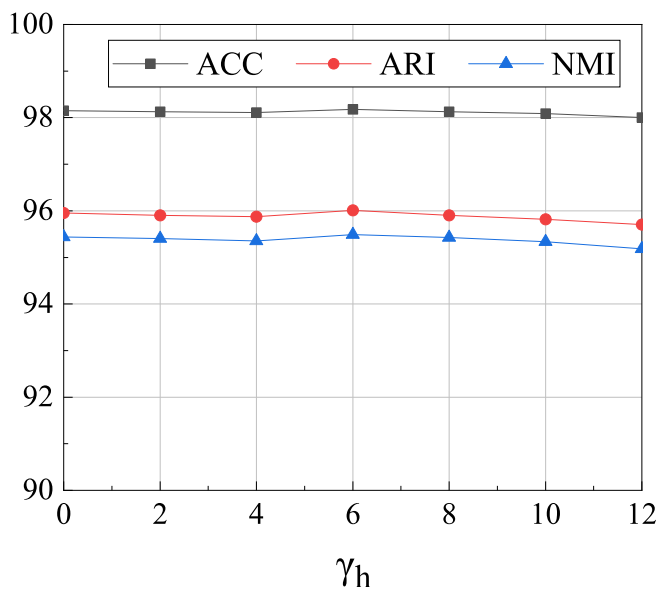


Figure 10: Sensitivity analysis of γ_r .

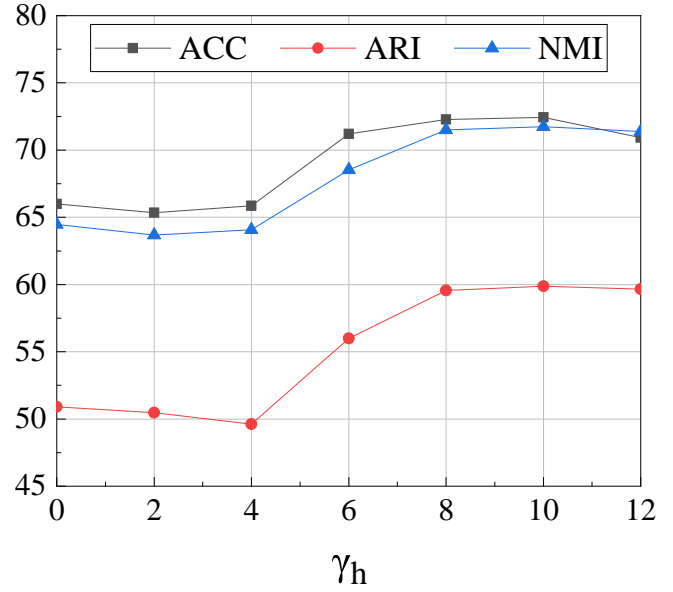
Sensitivity on hyperparameters τ_{ia} and τ_{pa} . τ_{ia} and τ_{pa} are the alignment temperature parameters to control the softness of the instance-level alignment and prototype-level alignment, separately. As shown in Figures 12 and 13, we can observe that the performances of our method remain relatively stable with changes to τ_{ia} , but exhibit significant changes with variations in τ_{pa} .

Compare with Zero-shot Learning

We compared MCA with two zero-shot learning methods, i.e., CLIP and MUST. Compared to CLIP, MUST improve CLIP by 3.3% on Caltech101 and 18% on UCF101. When compared to MUST, our method deteriorates MUST by -8.2% on Caltech101 and -8.5% on UCF101. Although the results show that our method performs worse than CLIP and MUST, our method has the advantage of not requiring class names as input, which is necessary for zero-shot learning. This makes our approach more versatile and applicable to a broader range of real-world scenarios.

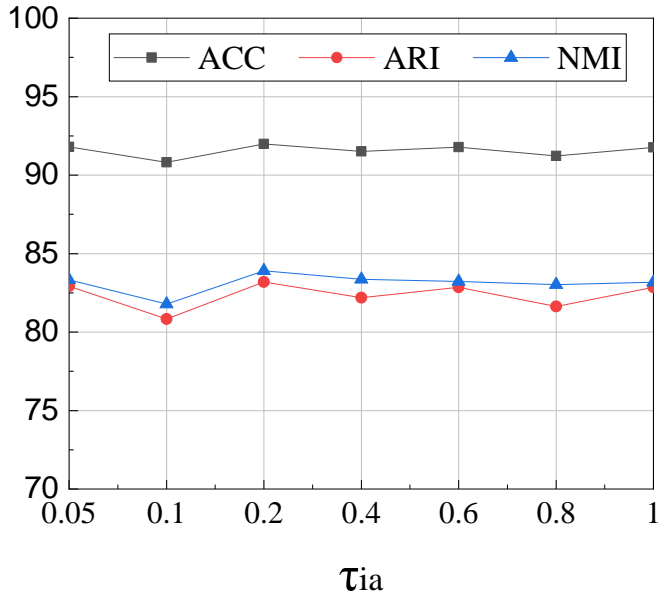


(a) γ_h on STL10.

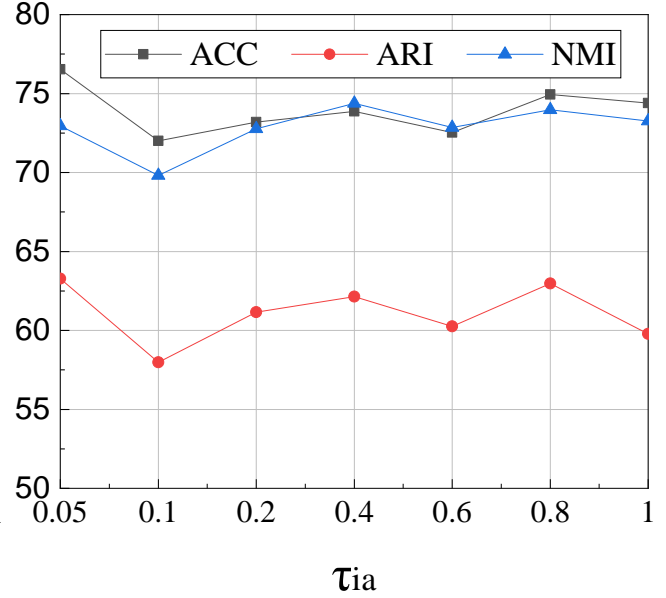


(b) γ_h on Imagenet-Dog.

Figure 11: Sensitivity analysis of γ_h .



(a) τ_{ia} on Cifar10.



(b) τ_{ia} on ImageNet-Dogs.

Figure 12: Sensitivity analysis of τ_{ia} .

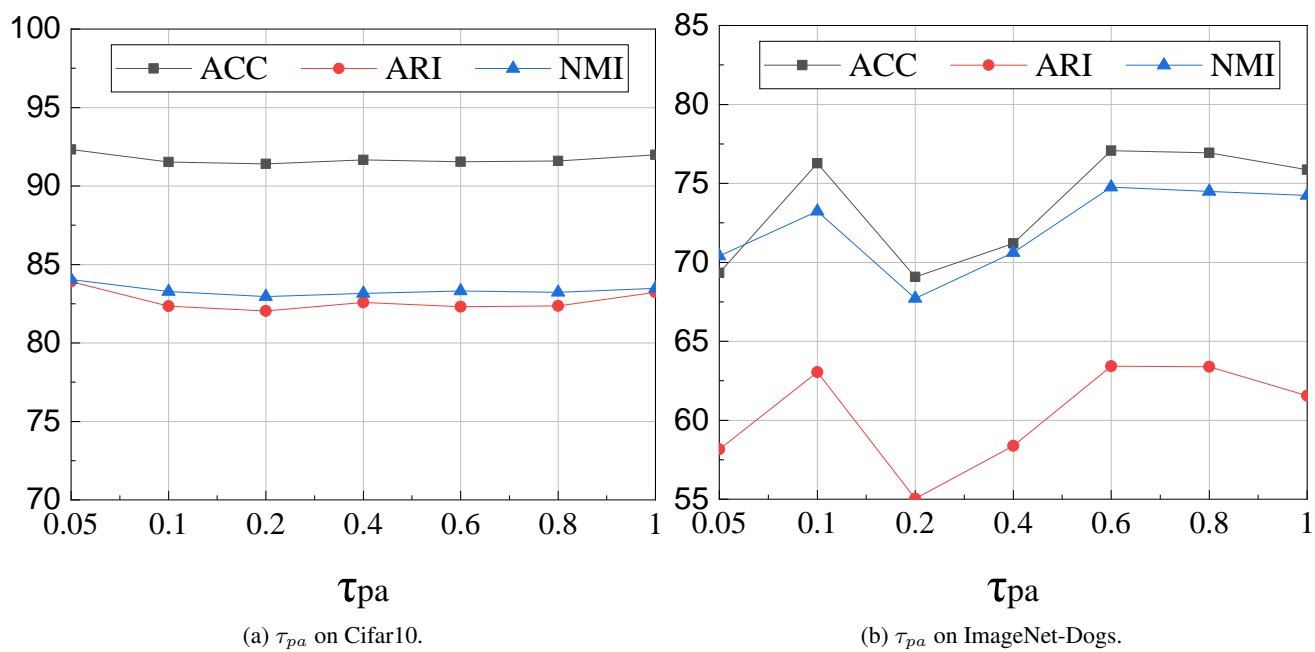


Figure 13: Sensitivity analysis of τ_{pa} .

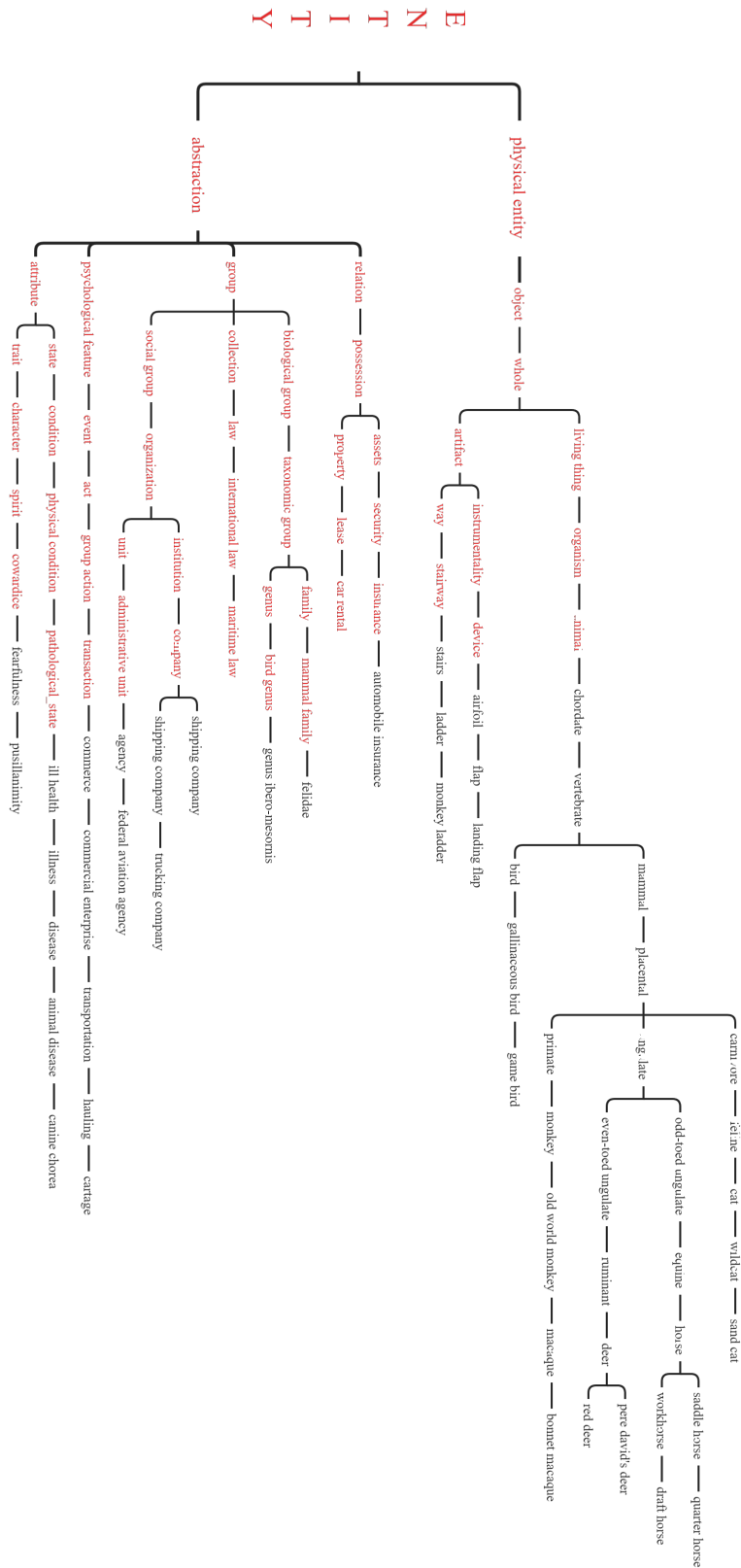


Figure 14: Example of hierarchy-based filtering result on STL10. The hierarchical semantic tree was built from WordNet (Miller 1995) and the top-6 levels of words in the tree (highlighted in red) were filtered.

